ISSUES WITH GRID INTEGRATION OF RENEWABLE ENERGY SOURCES

A DISSERTATION

Submitted in partial fulfillment of the
requirements for the award of the degree
of
MASTER OF TECHNOLOGY
in
ELECTRICAL ENGINEERING
(With specialization in Power System Engineering)

By

CHIRAG ANAND

DEPARTMENT OF ELECTRICAL ENGINEERING
INDIAN INSTITUTE OF TECHNOLOGY ROORKEE
ROORKEE - 247 667 (INDIA)
MAY, 2016

CANDIDATE'S DECLARATION

I hereby declare that this thesis report entitled **ISSUES WITH GRID INTEGRATION OF RENEWABLE ENERGY SOURCES**, submitted to the Department of Electrical Engineering, Indian Institute of Technology, Roorkee, India, in partial fulfillment of the requirements for the award of the Degree of Master of Technology in Electrical Engineering with specialization in Power System Engineering is an authentic record of the work carried out by me during the period June 2015 through May 2016, under the supervision of **Dr. Premalata Jena, Department of Electrical Engineering, Indian Institute of Technology, Roorkee.** The matter presented in this thesis report has not been submitted by me for the award of any other degree of this institute or any other institutes.

Date:

Place: Roorkee

Chirag Anand

CERTIFICATE

This is to certify that the above statement made by the candidate is true to the best of my knowledge and belief.

Dr. Premalata Jena
Assistant Professor
Department of Electrical Engineering
Indian Institute of Technology Roorkee

Acknowledgements

I would like to express my deep sense of gratitude and sincere thanks to my guide **Dr. Premalata Jena**, Department of Electrical Engineering, Indian Institute of Technology Roorkee, for her valuable guidance and support. I am highly indebted to her for her encouragement and constructive criticism throughout the course of this project work. Inspite of her hectic schedule, she was always there for clarifying my doubts and reviewed my dissertation progress in a constructive manner. Without her help, this thesis would not have been possible.

Chirag Anand

ABSTRACT

When renewable energy sources are integrated into the existing power system, then they act as a bridge between the electricity demand and supply, in a sustainable and greener way. But this grid integration poses certain challenges for the power system operator. In this work various issues, which are faced,are addressed. A typical IEEE 13 bus is used to simulate the microgrid environment. Among the various protection issues, high impedance fault(HIF) is addressed here. A high impedance fault(HIF) occurs whenever a conductor gets broken and touches ground or when a line comes in contact of a semi-insulating surface. Due to very small fault current, these faults are left undetected by conventional overcurrent relays. In this work, a technique based on Mathematical Morphology is implemented. Another technique based on the variation of 3rd and 5th harmonic current components is implemented. The fault direction is estimated using the fundamental apparent power. An anti-islanding detection technique, which discriminates between islanding and other events such as capacitor switching, load switching, based on positive sequence current and voltage components is proposed in this work. Another protection issue, which is considered here, is protection system blinding and sympathetic tripping. An adaptive protection scheme, based on the determination of optimal relay settings is implemented. A 5-bus system is simulated for this.

All simulations are carried out in real time(RSCAD) using real time digital simulator(RTDS).

Contents

List of Figures

List of Tables

Abbreviations

HIF	**H**igh **I**mpedance **F**ault
RTDS	**R**eal **T**ime **D**igital **S**imulator
DG	**D**istributed **G**eneration
NLP	**N**on **L**inear **P**rogramming
DER	**D**istributed **E**nergy **R**esource
DS	**D**istributed **S**ource
DFIG	**D**oubly **F**ed **I**nduction **G**enerator
VSC	**V**oltage **S**ource **C**onverter
MM	**M**athematical **M**orphology
CODO	**C**losing **O**pening **D**ifference **O**peration
DFT	**D**iscrete **F**ourier **T**ransform
PSO	**P**article **S**warm **O**ptimization

Chapter 1

Introduction

The power system is composed of different electricity generation units, devices which use this power generated and the power grid which connects the above two. The sole aim of this power grid network is to facilitate the transfer of electric energy from the point of generation to the point of consumption. Simultaneously, it needs to be ensured that the system reliability and voltage quality is maintained to an acceptable level, for both the producers and the consumers and that too for the lowest price possible. Till now, a lot of development have taken place in this regard. But there is still a large amount of research being done in this regard to make the functioning of power system even better. A sudden change on the side of generation or on consumer side could affect this situation of ours, to which we have become so habitual to.

There are many reasons for the introduction of renewable energy sources in the power system. Due to the deregulation of power system, in many countries, it is very easy for anybody to generate electric energy, through distributed generators, and export it the power system. The exact rules vary between countries, even the regulations for interconnection are different.

The main reason behind the introduction of renewable energy sources are environmental issues. Most of the conventional generation units emit carbon dioxide due to which global warming is a very likely consequence. Thus a shift from these conventional sources, which use fossil fuels to renewable energy sources will result in reduction in carbon emission. We can argue that Nuclear and hydropower units do not contribute to the carbon dioxide

emission but they still do have other environmental impacts, which cannot be neglected. One of these is the inability of ensuring a safe disposal of nuclear waste. Different countries are providing different incentives, to encourage the usage of renewable energy. The main impediment to development of renewable energy sources is the low cost of electricity production from conventional sources.

Another reason for this sudden shift towards renewable energy is that the difference between the highest consumption and the total capacity is very small. One solution is to build large conventional power plants, which is not acceptable as it requires huge investments and takes many years to complete. Small scale renewable energy sources do not have there limitations. They do require large initial investments, but these can be spread over many owners.

Whatever the reasons are behind the introduction of renewable energy sources, they still have to be properly integrated into the already existing power system network. With this new types of generation units, new problems occur which require some different solutions. Renewable energy sources are connected to the low or medium voltage distribution system, to which usually only loads are connected, no generation units. This makes the power flow in the distribution system bi-directional, which is traditionally uni-directional. This shift also affects the transmission and sub-transmission systems. The renewable energy sources are also referred by some other terms, such as "Distributed Generation", "Distributed Energy Sources" etc.

1.1 Issues with Integration of Renewable Energy Sources

It is not easy to determine what the main obstacles are with the integration of huge amounts of distributed generation/renewable energy sources to the power system. It is mainly determined by the local properties of the distribution system, by the kind of interface used and by the properties of the type of renewable energy source. Some of the impacts on the distribution level are as follows:

1. Various feeder and transformers could get overloaded due to large generation during the time of light loads.

2. There is an increase in the risk of over-voltages due to generation at remote parts of a feeder.

3. With the introduction of distributed generation, the power quality disturbance level may increase beyond the acceptable limit for the customers.

4. The protection devices may malfunction. That is, they might fail to operate or operate when not desired. The failure of the uncontrolled islanding operation is major impact on the protection scheme.

1.2 Literature Survey

A high impedance fault is the fault which occurs when an overhead conductor breaks or it touches a semi-insulating surface such as asphalt road, cement, tree or sand. Due to the high impedance, the fault current is not sufficient to be detected by the conventional overcurrent relays. After a high impedance fault, the energized conductor falls to the ground and this poses a threat to personnel. Sometimes arcing also takes place with these faults, due to which there is an additional risk of fire hazard.

The various detection methods for high impedance faults can be mainly classified into time domain and frequency domain algorithms, hybrid algorithms and expert systems. second-fourth and sixth harmonics [1]. In [1], a new detector is built. The detector was able to detect 100% faults, provided that the current due to arcing, at the point of fault is less than 5A. These were a few frequency domain based techniques. Another technique which improves upon the use of 3rd harmonics is reported in [2], [3]. In [2], low frequency current harmonics are measured and then compared with a week long data of the lower order harmonics at the substation. The conclusion was that the detection of high impedance fault is possible with the 2nd harmonic current. In [4], high impedance fault is detected using a combination of different peculiar characteristics. Another algorithm uses burst noise signal [5]. In this a technique is proposed for the detection of HIFs, accompanied by arcing, using burst noise signal, for the fundamental frequencies and lower order harmonics. Statistical techniques which use sequence components and their harmonics are used in [6]. Third harmonics are used for the detection of HIFs in [7]. The detection of HIFs is very important and some the reasons are mentioned in [8]. The detection of HIFs due to high frequency components is reported in [9].

In [10] three techniques for the detection of high impedance fault on a distribution system grounded at multiple positions is considered. The techniques are reviewed theoretically,

practical investigation is not done here. A prototype of the ratio ground relay is developed in [11]. Also the performance of the relay was further assessed using computer based tests. In [12], a laboratory setup of high voltage was built to study phenomenon of high impedance fault. The algorithm in it, makes use of the randomness in the fault current. The flicker in the current signal is obtained by comparing the positive and negative peaks, for each and very cycle with the ones in the next cycle. Under all the test conditions, except for the arc welder load, the algorithm performed excellently. In [13], the fractal techniques are used to analyze the properties of HIFs. During a HIF, the voltages and currents of a system change and a certain degree of chaos is introduced into them. This chaotic property is analyzed here. A new technique which uses superposition of certain frequency voltage signals is reported in [14]. The technique was proposed for radial distribution systems.

Wavelet analysis filter banks(WAFB) are used for the detection of HIFs in [15]. It helps in fast and accurate detection of HIFs. In [16], morlet waveforms are used for the detection of HIFs. This wavelet transform approach proves to be more efficient in monitoring fault signals with varying time. The use of discrete wavelet transform for the detection of HIFs in distribution systems is reported in [17]. In addition to this, frequency range and rms conversion is used and an algorithm based on pattern recognition is proposed. Some other time and frequency domain hybrid techniques are reported in [18]-[20].

In [21] different algorithms, using various parameters dependent on frequency, are employed. Final decision is made using an adaptive model, in which each algorithm is associated with weights. A similar technique is proposed in [22]. Here the arcing faults are distinguished form the normal system events using different protection algorithms. Another paper [23], proposes a practical detection scheme so that there exists a balance between fault detection and discrimination. This distinction becomes very crucial for low current faults such as HIFs. In [24], [25], Kalman filtering technique is used for the detection of HIFs. In [25], in addition to the Kalman filter, a support vector machine is also used. The applications of artificial neural networks(ANN) for the detection of HIFs by pattern recognition is reported in [26]. The technique reported in [27], based on ANN, performs well for HIFs having non-linear arcing resistance. Two new ANN based algorithms, for the detection of HIFs, are proposed in [28]. The algorithm works in multigrounded distribution networks, also in isolated, compensated and grounded, with a resistance of small value, distribution grids. In [29], mathematical morphology is

used for the detection of HIFs. The concept of mathematical morphology is explained in [30].

When a DG is introduced into the system, then it acts as an additional fault current sources which results in an increase in the short circuit level and also changes the magnitude and direction of the fault current. Thus with the introduction of DGs, the protection devices face new problems such as protection system blinding, sympathetic/false tripping. In [31], the issues which arise with the introduction of DGs into the system are discussed. The impact on the system voltage is discussed and protection issues such as the rating of devices, recloser coordination etc are also reported. Some protection issues are also discussed in [32]. Based on the issues, some strategies are suggested and their benefits are also discussed. The problem of sympathetic tripping is studied in [33] and a solution is also provided for the same. The solution is for a UK distribution power network. In [34], the various renewable energy sources are discussed. Issues related to system reliability and protection are discussed.

The adaptive protection is the main concern for the protection strategy. It is basically the self tuning of the relay according to the changing system configuration. In [35], a protection strategy is proposed to overcome the protection issue, when distributed generation is integrated into the distribution systems. For the optimal settings of the relay, non linear programming(NLP) methods are used. A modified particle swarm optimization technique is used in [36]. Another technique of relay setting optimization is proposed in [37].

Sometimes, due to technical problems, the switch connecting a microgrid to the main power system is opened automatically in order to isolate faults or this can also be done manually to eliminate some problems. There are two types of island operation, namely- short time or long time island operation and sustained island operation. A sustained balance of the reactive and active power between generation and consumption is required for the later case. Without very efficient control circuitry, such balance cannot be achieved. The possibility of a short time islanded operation occurring is more [38]. In [39], some results are presented which shows the time of operation of the short islanding operation. In [40], the effect of the DG islanding on the performance of the power system is reviewed. The relaying requirements for the islanding operation are reported in [41]. A new method which is based on the rate of change of power at the generator's terminals is introduced. In [42], a new anti islanding detection scheme based on power line signaling is proposed. The evaluation of the scheme was done using field

tests and simulations. The voltage unbalance at the terminals of the DG, is monitored in [43] for the detection of islanding.

1.3 Energy Scenario in India

The most starking feature of th Indian power sector is its diversity. The generation sources range from conventional sources like coal, hydro, natural gas and nuclear to the non-conventional ones like wind, solar, biomass etc. The demand for electricity in India is continuously increasing and to make sure that this demand is met, huge additions are required to the generation capacity.

As of April 2016, the total installed generation capacity in India stands at 302.833 gigawatts(GW) [44]. Of this total capacity, thermal power generation accounts for 211.42 GW. Hydro power generation stands at 42.783 GW, nuclear at 5.78 GW. The total generation from renewable energy sources is 42.849.

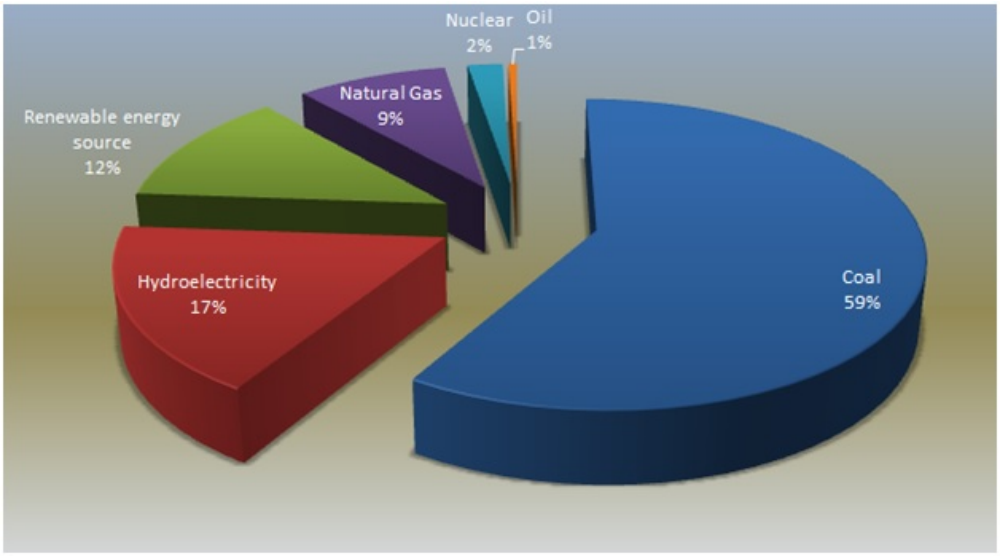

FIGURE 1.1: Energy Diversification in India

Fig.(1.1) shows the contribution of the various energy sources in the total installed capacity. The total generation from wind power is 26.866 GW, from solar power it is 6.762 GW and the rest is mainly from bio-power and small hydro power. This shows that the major contribution of the renewable energy comes from solar and wind power. The situation is similar in many other countries of the world. There is a large difference between the total generation from renewable energy sources and the total potential.

1.4 Organisation of Report

This report is organized as follows: Chapter 2 includes a description of microgrid and various renewable energy sources. Chapter 3 consists of a detailed discussion on issues addressed in this work. This includes HIFs and un-controlled islanding. It also includes protection system blinding and sympathetic tripping. The system is described in Chapter 4. Chapter 5 describes the HIF detection technique and the adaptive protection scheme. The proposed anti-islanding detection technique is also described. Chapter 6 consists of the results, which are followed by conlusion in Chapter 7.

Chapter 2

Microgrid and Renewable Energy Sources

2.1 Microgrids

Microgrid is a cluster consisting of loads, distributed generation and storage devices, which can function efficiently under both conditions, grid connected and islanded mode. Distributed generation and distributed storage can be clubbed under distributed energy resource(DER). The structure of the microgrid is such that the loads and energy sources, can be easily connected and disconnected to the utility without much disruption to the rest of the system and the microgrid itself.

Both the utilities and the customers have their own sets of benefits from a microgrid. For the customer, with the advent of a microgrid the reliability of power is increased during an outage on the utility side. In addition to this, quality of power supplied is improved, by reducing the total harmonic distortion(THD) at the loads. For the utilities, overload problems are resolved by removing a load from the grid. This is done by intentionally islanding a part of the grid. A microgrid also facilitates easy maintenance of the utility. Before going for a microgrid, there needs to be thorough planning done, so as to avoid any problems.

For proper functioning of a microgrid, a switch needs to be opened and the DER should be able to deliver all the power that is required by the loads in the islanded section.

This is ensured when a suitable frequency and voltage levels are maintained for the loads in the islanded section. There are short interruptions, which occurs when there is a transfer from grid connected to islanded mode. This interruption depends on the technology of the switch used. Whenever there is a power loss then the DER, which is assigned the job to provide power to the islanded loads, must restart and take care of the island load after the interconnecting switch is opened. There needs to be a proper power flow analysis of the islanded microgrid. This is done in order to make sure that the voltage regulation is maintained at acceptable levels. When the utility side power is restored, then the switch must not reclose instantly, unless both the islanded and utility portions are in synchronism.

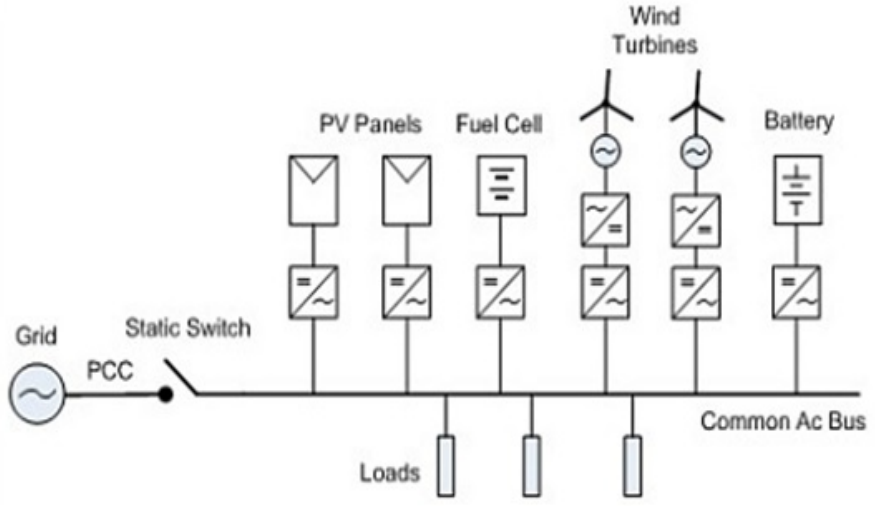

FIGURE 2.1: Microgrid Diagram

Microgrid consists of: distributed storage, distributed generation, interconnection switch and control systems. The main problem is the design of the low cost technologies for the installation and usage of the microgrids. Fig.(2.1) shows the general architecture of a microgrid consisting of switch, DGs, distributed storage and loads, as mentioned above.

Distributed generation(DG) are small enery sources which are positioned near the loads, i.e. near the point where the power is to be used. Generally the technologies involved in a DG are photovoltaic, fuel cells, wind, microturbines etc. These technologies may be driven either by fossil fuels or by renewable energy fuels. The various renewable energy sources are discussed in the next section. Another type of DG is combined heat and power, which basically utilizes the heat energy generated by another sources and converts it into power. Nowadays, many DGs are interfaced with the system using power

electronics components. The power electronics components also perform some protective functions, for the DGs and the local grid. This facilitates easy disconnection and reconnection with the grid. The power electronics interface, increases the performance of the DG. Without a power electronics interface, the DG will simply have a set of protective relays and switches for the safe interconnection with the grid.

Distributed storage(DS)is used in those microgrids, where the generation capacity and the total connected load, are not exactly same. This acts as a bridge in fulfilling the energy needs of a microgrid. The time for which the normal energy capacity can serve the load at rated power, is known as the storage capacity. Storage capacity can be grouped in terms of the energy density requirements and the power density requirements. Energy density is for medium and long term needs while power density is for very short and short term needs. The overall performance of the microgrid is enhanced, with the introduction of distributed storage, in the following ways:

1. It makes sure that the DGs run at constant speed providing a stable output, even with variations in the loads.
2. It increases the ride through capability, i.e. the microgrid is allowed to function properly even when there are variations in the primary energy sources(like sun for solar, wind for wind power system etc).
3. It allows the DGs to operate continuously like a dispatchable unit.

The interconnection switch acts as the point of common coupling between the main power system to the microgrid. With the advent of technologies in the field of power electronics, this task is now consolidated by them, which was earlier being carried out by protective relays. The operating conditions are continuously measured on both the utility and the microgrid sides of the switch with the help of current and voltage transformers.

The last component is the control system. Its functioning is critical to the operation of a microgrid. It ensures the safe operation of the system in both the grid connected and the islanded modes. The control system of a microgrid may be a central controller or there may be small control systems for each DG. With the disconnection of the microgrid from the utility, the control system has the task of controlling the local voltage and frequency, provide or absorb the real power difference between the generation and loads present

in the microgrid, exactly match the reactive power generated and that required by the load and also protect all the components of a microgrid.

2.2 Renewable Energy Sources

The renewable energy domain, currently, is dominated by wind and solar power. Apart from them there is Combined Heat and Power(CHP), small hydropower, Geothermal power, Tidal power. All these are discussed briefly in this section, with the emphasis on wind and solar power.

2.2.1 Wind Power

The kinetic energy of the air(wind), due to its horizontal displacement, is converted into the kinetic energy of the turbine rotation. This is done with the help of a number of blades connected to an axis. After this stage, there is another conversion from the rotational energy of the turbine into electrical energy with the help of an electric generator. There were different technological proposals over the years, which have been used to produce electricity from wind power. The predominant technology, currently, is a two- or a three- blade turbine with a horizontal axis, on the mechanical side. There are three technologies, currently competing for the conversion into electrical energy, namely:

1. Directly connected induction generator.
2. Doubly fed induction generator.
3. Generator with a power electronics converter.

2.2.1.1 Properties

Wind power generation varies with the variation of the primary source i.e. wind or more specifically wind speed. The variation is over a wide range of time, from less than a second though seasonal variations. Due to the strong variation of power generated, from solar and wind, with time, this type of generation is also termed as intermittent generation. The predominant concern for the power system is not only this variation with time but also how accurately this variation can be predicted. Due to the difficulty in prediction of wind speed, longer than a few hours, the wind power is also difficult to

be predicted. But over larger areas, these predictions become better. This is the only thing which matters at the transmission level.

2.2.1.2 Power Generated v/s Wind Speed

Fig.(2.2) shows the curve of the amount of power generated by the wind system as the wind speed is varied. The curve between power generated and wind speed show four distinct regions, which are as follows:

1. There is no power generated until the wind speed reaches a threshold value. This speed is known as "cut in speed". This is because, below this speed, the kinetic energy of the wind is not sufficient to take care of the mechanical and electrical losses. For suppling these losses, energy from the grid would be needed and also to keep the blades moving. This speed is generally between 3 m/s and 4 m/s.

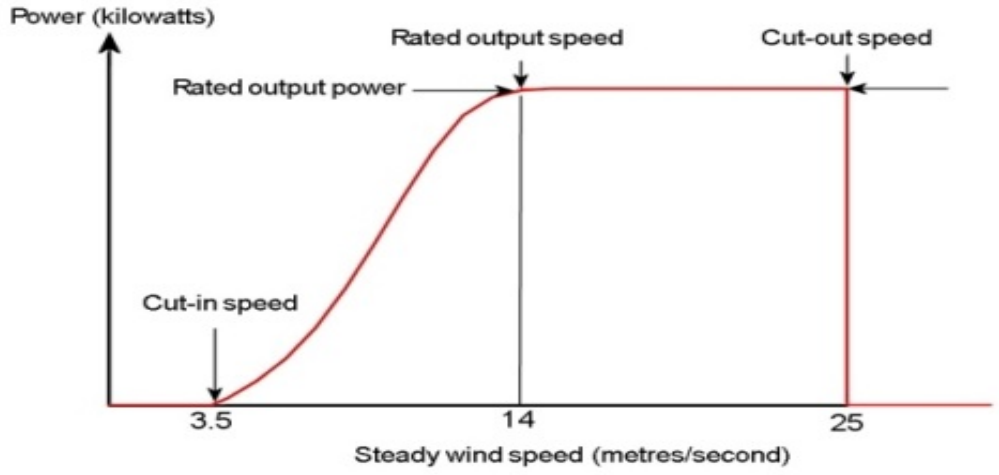

FIGURE 2.2: Generated Power as a function of the Wind speed

2. In this second region, the power generated increases with the increasing wind speed. For a particular wind speed, the turbine produces its maximum power in this region. The amount of energy produced is directly proportional to the cube of the wind speed. This relation is the predominant cause of the fast rise in the generated power. With large variations in wind speed, in this region, there will be large variations in the generated power.

3. When the curve enters into the third region, the increase in the power generated, with the increase in wind speed, is less as compared to the previous region. Later on the power generated becomes constant or sometimes decreases also. This depends

upon the technology of the turbine used. The nominal power of the electrical installation is determined on the basis of the turbine rating. This sets the limit to the maximum amount of power which can be generated. At around 10.5 m/s to 14 m/s, 90% of the rated power is obtained. The wind speed at which the rated power is obtained is termed as the rated speed.

4. With the further increase in wind speed, generally beyond 25 m/s, the power generated becomes zero. This is because blades are not allowed to move, in order to protect them from damages caused by the high mechanical forces due to high wind speeds. The speed at which this phenomenon occurs is know as "cut out speed".

2.2.2 Solar Power

The total amount of energy which $1m^2$ of the surface of earth receives varies from one location to another. With a clear sky, it is lowest at the poles and highest near the equator. When the presence of clouds is considered then the amount is highest in the deserts.

The energy which is received from the sun can be utilized in a number of ways. The predominant use of this energy today is in the form of solar panels, which are often installed on the rooftops of the buildings. One of the major advantages of this type of solar power generation is that the generation is close to the consumption, almost at the same point. Large solar power plants are not based on photovoltaics but instead on concentrating solar thermal plants, where the sunlight is focused using large array of mirrors. This concentrated sunlight is used for boiling water which is further used to power a turbine just like in conventional thermal plants. The main advantage of concentrating solar plants over photovoltaics is that the former is much cheaper. Concentrating solar is more preferred at those places where land is easily available. Photovoltaics prove to be beneficial in built-up areas, as it needs less space. Solar power is used in another aspect, as a means to directly heat water and this is referred to as solar thermal. This takes care of the hot water requirements of a household. This is not directly connected to the grid, so the problems arising due to integration are not there.

The total amount of solar radiation that reaches the solar panel decides the amount of electrical energy which will be generated by the photovoltaic installation. This amount

of radiation is known as 'irradiation' or 'insolation'. This irradiation can be of three different types, namely:

1. Direct Irradiation- which reaches the solar panel directly. This depends on the angle between the panel and the sun.
2. Indirect Irradiation- Also referred as diffused or scattered irradiation. This indirect irradiation is the one which comes from the sky and it varies very slowly with the variation of the cloud cover in the sky.
3. Indirect Irradiation from the earth. It depends on the direct irradiation in nearby places. With increase in cloud cover, this type of irradiation decreases.

2.2.2.1 Properties

The total amount of solar power which will be generated by a solar power installation depends on position of the sun and the cloud coverage. The cloud coverage variations are similar to the one observed in wind speed. The cost per kilowatt of the electricity generated, remains same with increasing size. Thus rooftop solar installations are an economical option.

The variation of solar power in a day shows that the peak occurs around noon. It is advised that the solar panels are kept facing southeast or southwest(placed in northern hemisphere), to make sure that the peak in generation and load occurs at the same time.

The variation over a year suggests that the peak occurs in summers. During this time, in hot countries, the demand is also highest. But the daily peak and annual peaks in load does not coincide with the time at which the sun is at the highest point in the sky. Despite all this, solar power is expected to offer some contribution to the peak demand. The solar panels can be tilted in such a way so that their contribution to the peak load is maximized.

2.2.3 Combined Heat and Power(CHP)

This type of generation process is also known as cogeneration. This type of generation uses heat which is exhausted from another generation unit and applies it for further process requirements. The energy utilization of the complete unit it improved due to this. CHP does not have to include any renewable source of energy. Instead there are

many CHP units which use natural gas as the primary source. CHP units using biomass are the only renewable form.

The total generation capacity depends directly on the heat demand. With the increase in the heat demand, the generation capacity increases. The heat, which is the by-product of electricity generation, sets a minimum threshold to the generation of electricity. With large number of industrial installations, the heat demand has become quite predictable and constant. In case of usage of CHP for room heating, either in an industry or offices or for domestic usage, the heat demand depends on various weather parameters: difference of the room temperature with the outside temperature, irradiance and wind speed. All these parameters are not easy to predict, therefore the generation from CHP cannot be predicted accurately.

2.2.4 Hydropower

The energy in the water flowing, towards the sea, is utilized for the generation of electricity in hydropower. The most predominant form is by constructing large dams to create reservoirs. The potential energy difference is created due to the difference in the level of water, upstream and downstream. The rating of these installations can be as high as hundred of MWs or as small as a few tens of MWs. Many such large units are already in operation.

Hydropower sources of energy, which consists of large reservoirs are located in remote areas. These large hydropower units need a strong transmission system. Therefore if the plan is to increase the amount of generation from hydropower units, then the transmission system also needs to be strengthened. The run of river and other small hydropower units could be located close to the customers but their location is still restricted to the mountainous region. The distribution grid in the mountain region can be strengthened using these small hydropower units.

2.2.5 Tidal Power

The energy difference between a high and low tide or the water flow between high and low tide is utilized to generate electricity in case of tidal power. One scheme uses the difference between sea level of high and low tide and the other scheme uses difference between the water flow of high and low tides. At places where there is a large difference

between the low and high tides, former scheme is preferred and where there is a strong water flow, the later one is preferred.

2.2.6 Geothermal Power

Geothermal energy is the energy from the earth's core. Heat is continuously generated inside the earth's core and this heat is utilized to heat buildings or for the generation of electricity. Energy can be done either mechanically or in other cases the heat is used directly. The temperature inside the earth's surface is higher than that of the sun. The country with the highest usage of geothermal power is Iceland.

Chapter 3

Different Issues due to Grid Integration of Renewable Energy Sources

---

3.1 High Impedance Faults

A high impedance fault is the fault which occurs when an overhead conductor breaks or it touches a semi-insulating surface such as asphalt road, cement, tree or sand. The predominant need to detect these kinds of faults, despite very low fault currents, is that they pose serious threat to the safety of the public and also there is a risk of fire. The main characteristic of an HIF is that the fault impedance is very high such that the fault current is not detected by the conventional overcurrent relays and fuses. The low impedance faults have very high fault currents and therefore they pose serious threat to the power system equipments. This is not the case for HIF, i.e. they do not cause any damage to the power system equipments.

3.1.1 Limitation on HIF detection

There are many different methods for HIF detection. But no technique is able to detect all HIFs. For example take the case of the situation when a conductor at the end

of a feeder falls to the ground after breaking. The fault current in this case is very small due to which it becomes difficult for any detector to sense this. The motive is to detect all HIF events and simultaneously be unaffected from all events un-related to HIF. Practically it is not at all possible to detect all HIFs and it is also impossible to achieve a high degree of immunity against false outputs. This is due to the probabilistic characteristics of HIFs. To go in the direction of installing a close to perfect system is not cost effective. When an energized conductor is left on the ground, it poses an increased hazard to the public, which is present in the vicinity of the conductor. Thus the solution is- use HIF detection and clear the fault immediately. But the process is not that simple. The type of HIF detection available currently is not very fast. Therefore the ability to protect and prevent against an injury due to the downed conductor is very limited.

3.1.2 HIF Characteristics

Two main features of a HIF are arcing and very low fault current. By default, HIFs produce very small or no fault current. In addition to this the waveform of the fault current is very erratic.

Also, adding to the low value of fault current, HIF is characterized by erratic behavior with very unstable and wide fluctuations in the HIF fault current. The fault current is composed of both lower and higher order harmonics.

The predominant voltage levels at which HIFs occur is 15kV and below, with the worsening of the situation at lower voltages. At voltages of more than 25kV, the problem becomes less severe, but the possibility of HIFs is still there. Generally, the detection technique for HIF is designed keeping in mind the voltage levels of 15kV and below distribution circuits. There are also some other cases, where the detectors are useful at a higher voltages also.

HIF detectors are designed only for overhead lines and not for underground cables, as the public safety issue is not present in the later case. The new overhead systems which have large conductors and neutrals are less prone to HIFs caused by wire breakage. Older systems are more prone to this event and thus HIFs are more likely to occur there.

3.2 Protection System Blinding and Sympathetic Tripping

3.2.1 Protection Blinding

Traditionally, there is only one source of power which contributes to the fault current in a distribution system. But with the integration of DGs new sources of fault currents come into the picture. This not only increases the short circuit level but also alters the direction of fault current. In addition to this, if a synchronous DG is added then the fault current which is contributed by the upper DG gets decreased. This effect is known as protection blinding and is also known as protection under-reach.

Consider a symmetrical fault at bus 2. The fault current, with DG connected, which flows from the grid is less than the fault current which flows when there is no DG. Due to this the initial reach of feeder relay gets reduced. The issue of protection blinding can be quantitatively analyzed.

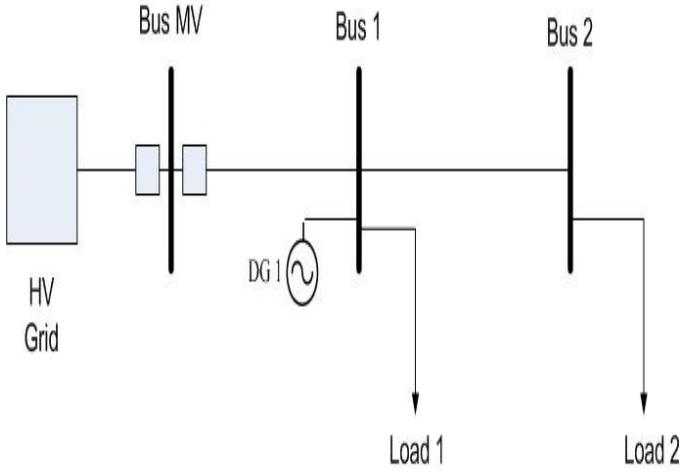

FIGURE 3.1: Protection system blinding illustration

Z_{sys} is the impedance upstream of the grid. Z_L is the impedance of the line between bus 1 and 2 and the impedance inserted by the DG is Z_{DG}. Now the fault current before and after the connection of the DG is given:

$$I_{f,tot}^{noDG} = I_{f,sys}^{noDG} = \frac{V_f}{z_{sys} + Z_L} \tag{3.1}$$

$$I_{f,tot}^{withDG} = \frac{V_f}{Z_L + \frac{Z_{sys} * Z_{DG}}{Z_{sys} + Z_{DG}}} \tag{3.2}$$

It can be seen from the above two equations that $I_{f,tot}^{withDG} > I_{f,tot}^{noDG}$. The total current from the DG and the system is given by the following equations.

$$I_{f,sys}^{withDG} = \frac{V_f}{Z_{sys} * (\frac{Z_L}{Z_{DG}} + 1) + Z_L} \tag{3.3}$$

$$I_{f,DG} = \frac{V_f - Z_L * I_{f,sys}^{withDG}}{Z_L + Z_{DG}} \tag{3.4}$$

From eq.3.1 and eq.3.3, $I_{f,sys}^{noDG} > I_{f,sys}^{withDG}$.

Now the DG and the line impedances are expressed in terms of the system impedance. Thus let $Z_{DG} = m * Z_{sys}$ and $Z_L = n * Z_{sys}$. Also let k be the ratio of the current contribution from the mains, with and without the connection of DG and l be the ratio of the entire fault current with and without the connection of DG.

$$k(m,n) = \frac{I_{f,sys}^{withDG}}{I_{f,sys}^{noDG}} = \frac{m + m * n}{m + n + m * n} \tag{3.5}$$

$$l(m,n) = \frac{I_{f,tot}^{withDG}}{I_{f,tot}^{noDG}} = \frac{(m+1) * n + m + 1}{(m+1) * n + m} \tag{3.6}$$

If we take n as constant, then with decrease in the value of m, k increases, i.e. the large the DG capacity, the lower is the current contribution from the mains. With m fixed, as the location of fault is going down the feeder, increasing n, the contribution from the main decreases. As Z_{DG} and Z_L decreases, the total fault current value decreases.

3.2.2 Sympathetic Tripping

Sympathetic tripping is the unwanted operation of a feeder relay, due to the current from a DG for a fault which is outside its zone of protection. This is also known as false tripping. Like protection blinding, sympathetic tripping also occurs mainly in distribution systems. Consider the system. A three phase fault occurs at bus 2 and let the impedance of feeder 2 be denoted by Z_{L2}.

$$I_{f,tot}^{noDG} = I_{f,sys}^{noDG} = \frac{V_f}{Z_{sys} + Z_{L2}} \tag{3.7}$$

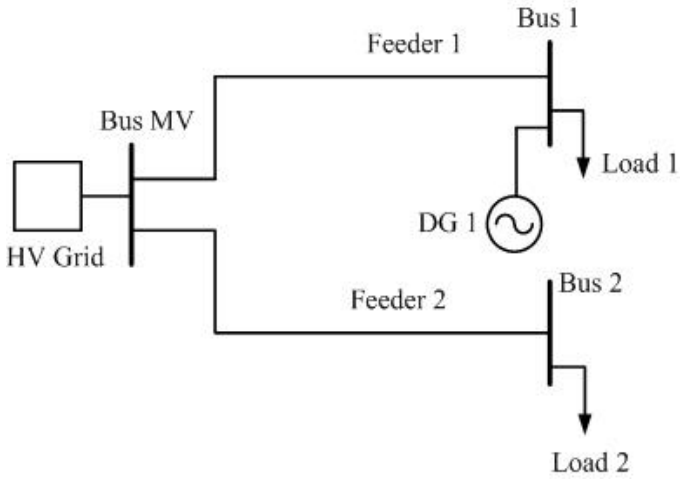

FIGURE 3.2: Sympathetic tripping illustration

$$I_{f,tot}^{withDG} = \frac{V_f}{Z_{L2} + \frac{Z_{sys} * Z_{DG}}{Z_{sys} + Z_{DG}}} \tag{3.8}$$

The fault current contributions from the mains and the DG are shown below.

$$I_{f,sys}^{withDG} = \frac{V_f}{Z_{sys} + (1 + \frac{Z_{sys}}{Z_{DG}}) * Z_{L2}} \tag{3.9}$$

$$I_{f,DG} = \frac{V_f}{Z_{DG} + (1 + \frac{Z_{DG}}{Z_{sys}}) * Z_{L2}} \tag{3.10}$$

It can be seen from the above equations the current from the mains and DGs increases as the fault gets closer to the substation. Let r be the ratio fault current from the DG to the total fault current.

$$r(m,n) = \frac{I_{f,DG}}{I_{f,tot}^{withDG}} = \frac{m + n + m * n}{(m+1) * m + (m+1)^2 * n} \tag{3.11}$$

If m tends to zero, then r tends to 1. This is the case when the DG impedance is negligible in comparison to the mains. It can be said that with increase in the capacity of the DG, the possibility of sympathetic tripping increases.

3.3 Islanding

Islanding is said to occur when a part of the distribution system gets isolated from the power system but it still continues to be energized by a DG. Islanding can be of two types, controlled and uncontrolled. The main cause of concern is uncontrolled islanding,

which needs to be detected. With the integration of DGs, the assumption that the distribution system will not get any power in case of a fault in the transmission system is no longer valid. The main drawbacks of un-intentional islanding are:

1. Voltage and frequency may not stay which the desired limits.
2. It can cause danger to the safety of line repair crews.
3. It may cause power quality problems.
4. Islanding interferes with the functioning of inverters. Many DGs are interfaced to the main grid with inverters.

Islanding detection techniques are of two types:

1. Passive Islanding detection This method uses the voltage, current and frequency at the DG for the detection of islanding. They constantly measure these values in the system. The value of the voltage, current and frequency changes when an islanding operation takes place. This helps in discriminating this from other events.
2. This includes continuous communication between the DGs and the utility to check the status of power supply. These techniques can detect islanding, even when the generation and load are balanced.

Chapter 4

System Description

In this work, two different systems are simulated in RTDS. And IEEE 13 bus system used, which is used for HIF and islanding detection. Another is a 5 bus system used for optimization of the relay setting, in order to negate protection system blinding and sympathetic tripping. An IEEE 13 bus system is constructed in RTDS, in order to simulate a microgrid environment with both wind and solar power generation units. DG1 denotes the wind generator, interfaced to the grid through at BUS 675. A doubly fed induction generator is used. DG2 denotes the solar power generator. It is interfaced to the grid at BUS 645 through a power electronics inverter.

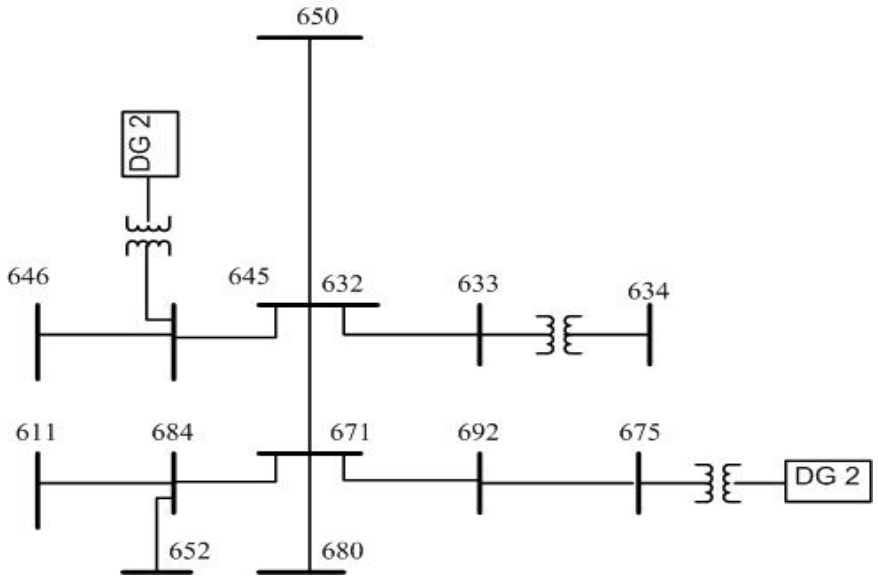

FIGURE 4.1: IEEE 13 bus microgrid

There are various loads connected in the system. The point of common coupling between the main grid and the microgrid is at BUS 650. The wind and solar power, both are of 2 MW rating. The total load in the system is 5.211 MW. The different system components are as follows:

1. Source
2. Wind power
3. Solar power
4. Load
5. High Impedance Fault model

The wind system is integrated at bus 675 and the PV system at bus 645. The wind system uses a doubly fed induction generator(DFIG) for conversion of mechanical energy into electrical. The frequency of the system is 50Hz. The nominal voltage of the system is 4.16Kv. The detailed description of the wind and solar power systems is given in the subsequent sections.

4.1 Wind System

The wind system used here consists of a doubly fed induction generator(DFIG). It is currently the most attractive option for all the utilities because of its ability to provide reactive power to the system during its operations in low voltage conditions. Another advantage of DFIG is that it can extract the maximum wind energy over a wider range of wider range of wind speeds. The fixed speed induction generators does not have this advantage. The DFIG employs an AC-AC converter in its rotor circuit , known as Scherbius Drive. This type of configuration has become a norm for high power applications where a limited speed range is involved. The power converter is to be rated only for the rotor power. The rotor windings are wound for three phases. They are fed from two pulse width modulated(PWM)(voltage fed, current regulated)inverters which are connected back to back. The connection with the rotor windings is made through slip rings. The voltage source converters(VSC) bridges are named as grid and rotor VSC. The major advantages which the Scherbius scheme provides are as follows:

1. The rotor speed is allowed to vary across all the regions i.e. above, below and through synchronous speed.

2. The rotor can also operate at synchronous speed, if DC current is injected into the rotor.

3. The stator and rotor currents have less distortion.

4. The rotor torque, as well as the excitation current can be controlled independently with vector control in the rotor VSC.

5. With the vector control the power factor and therefore both the real and reactive powers from the supply can be controlled independently.

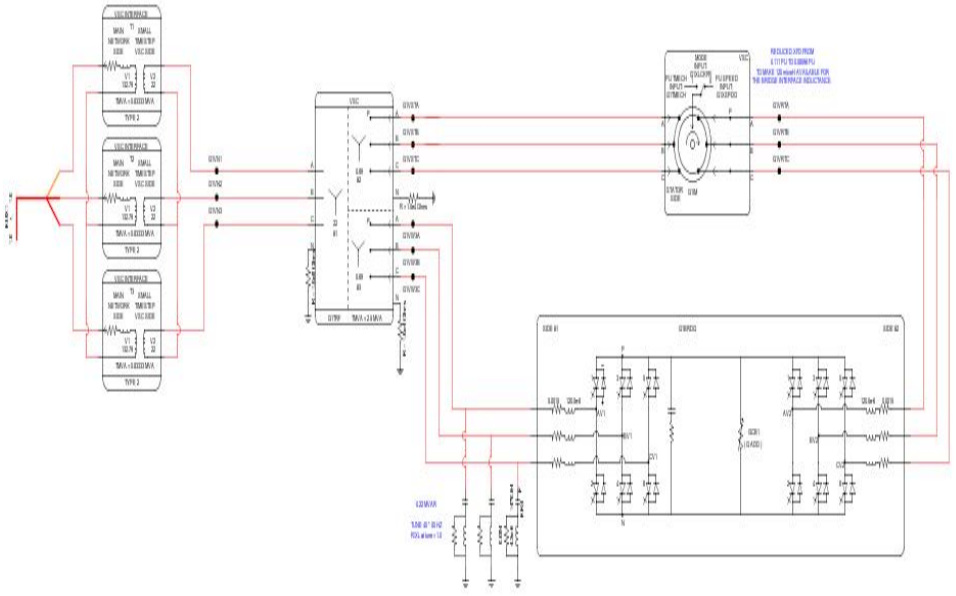

FIGURE 4.2: Wind Generator

From the above figure, it can be seen that the stator is directly connected to the grid and rotor through a back to back voltage source converter. The list of the components in the Wind system are as follows:

1. Doubly fed induction generator(DFIG).

2. Grid Voltage source converter(VSC).

3. Rotor Voltage source converter.

4. Filter.

5. Interface Transformer.

6. Crowbar Control.

7. Wind turbine.

All these components are described in the following sub-sections.

4.1.1 Doubly Fed Induction Generator

In this work DFIG is used, which is capable of variable speed operation. The key advantages offered by DFIG are as follows:

1. Mechanical stresss are reduced by absorbing gusts of wind. The mechanical inertia of the turbine is used to store energy, which creates an elasticity that helps in reducing torque pulsations.

2. They also improve system efficiency. Turbine speed can be adjusted as a function of wind speed in order to maximize the power output.

3. Acoustic noise is reduced. This is due to the fact that with a DFIG low speed operation is feasible during low power situations.

4. Reactive power can also be generated with a DFIG.

5. The torque and power pulsations, which are caused by back pressure of the tower are compensated dynamically by DFIG.The rate of torque pulsations is equal to the speed of the turbine times the number of rotor wings.

4.1.2 Grid Voltage Source Converter

The Grid VSC maintains operates in such a manner so that a constant voltage is maintained across the capacitor while the rotor VSC injects or extracts the current. The grid VSC is a current regulated bridge with the capacitor voltage being regulated by the real component and the terminal voltage by the quadrature component. By regulation of current, means to transform it from 3 phase to 2 phase and then apply this to a rotating reference frame. This is done in order to extract the ac fundamental component. The

resulting components of current are referred to as direct and quadrature currents. Each and every control component converts the engineering quantities into per unit on input. This allows for easy scaling of the controls for smaller or larger DFIG projects.

4.1.3 Rotor Voltage Source Converter

The principle of operation of the rotor VSC is very similar to that of the grid VSC. The rotor currents are converted to quasi dc quantity and is regulated by PI controls, using a rotating reference frame. The difference in the position of the stator flux vector and the physical rotor direct axis determines the rotating reference frame. The difference is constantly changing and is also known as the slip angle. After decoupling operation is performed and d and q rotor currents are obtained, it is very easy to independently control the rotor excitation current and the electrical torque. The rotor currents are converted to per unit by inverting them and then multiplying by 0.666. This is done to accommodate the transformation block of ABC to DQ. The optimal power reference computations help in determining the quadrature axis rotor reference.

4.1.4 Filter

The control components' performance is improved with the addition of the high pass filters. The rating of the filter was selected arbitrarily at 10% of the DFIG rating and the switching frequency of the PWM is the cutoff frequency of this filter. The design follows:

$$X_c = \frac{(0.69)^2}{0.22} = 2.164\Omega \tag{4.1}$$

$$C = \frac{1}{X_c * \omega} = 1.47mF \tag{4.2}$$

$$\omega_r = 40 * 50 * 2 * \pi \tag{4.3}$$

$$L = \frac{1}{(\omega_r^2 * C)} = 4.3\mu H \tag{4.4}$$

$$R = \omega_r * C \tag{4.5}$$

4.1.5 Interface Transformer

The interface transformer are used to tie the small time step network to the large time step. This transformer can also be used to change the scaling and can become larger in

terms of MVA and current ratings. If we are using a single wind generator, in order to represent an entire wind farm, then this interface transformer ratings can be changed to do so.

4.1.6 Crowbar Control

The crowbar is nothing but a shunt resistor, used for protection purposes, between the two VSC bridges. A switch in series with it is also placed. With the increase in capacitor voltage or when the rotor currents exceed beyond their limits, then the switch is closed and it brings down the voltage across the capacitor. The increase in current and voltages is generally due to external faults in the AC side of the system.

4.1.7 Wind Turbine

The model for the wind turbine in RTDS combines the DFIG and the multimass model. The wind turbine model calculates the mechanical torque, speed is calculated by the multimass and the DFIG is used to calculate the electrical torques.

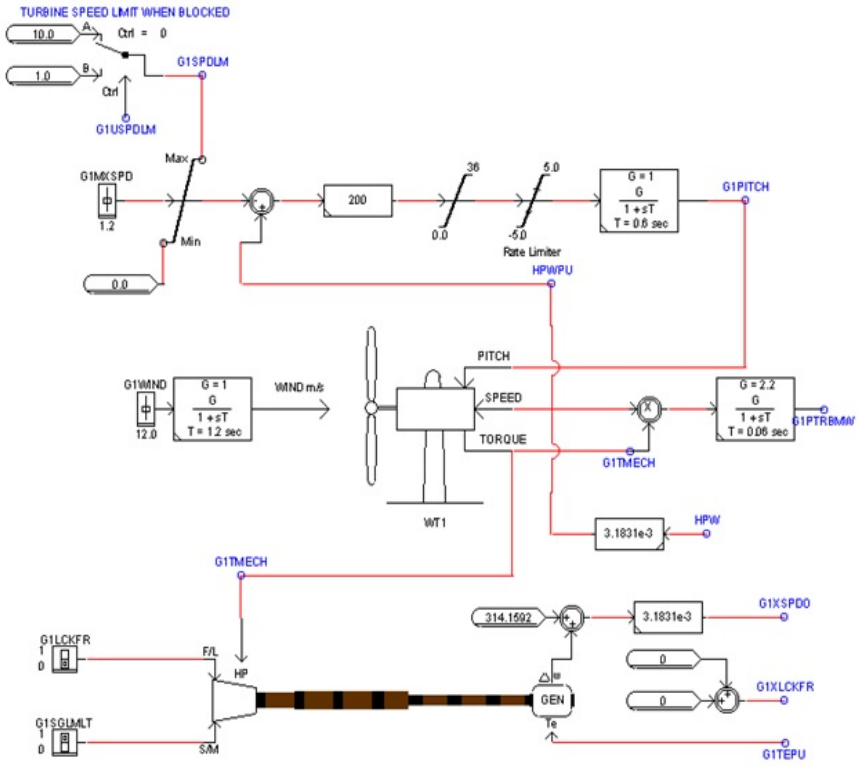

FIGURE 4.3: Wind Turbine

The wind turbine which is used here acts as the one having a variable speed pitch control. When the electrical and the mechanical systems are in resonance with each other, then this leads to torsional oscillations in the system which causes additional stresses to the mechanical couplings, which are there between the various turbines and those between the turbine and the generator. The pitch of the wind turbine is controlled so that maximum power is obtained.

4.2 Solar Power System

In order to build a PV module, solar cells can be connected either in series or in parallel to each other. Normally a module has 36/72 cells connected in series. The PV modules are further combined in series and parallel, forming PV arrays. When we combine these individual solar cells into PV arrays, then large and wide ranging values of voltages and currents are achieved at the terminals of the PV array.

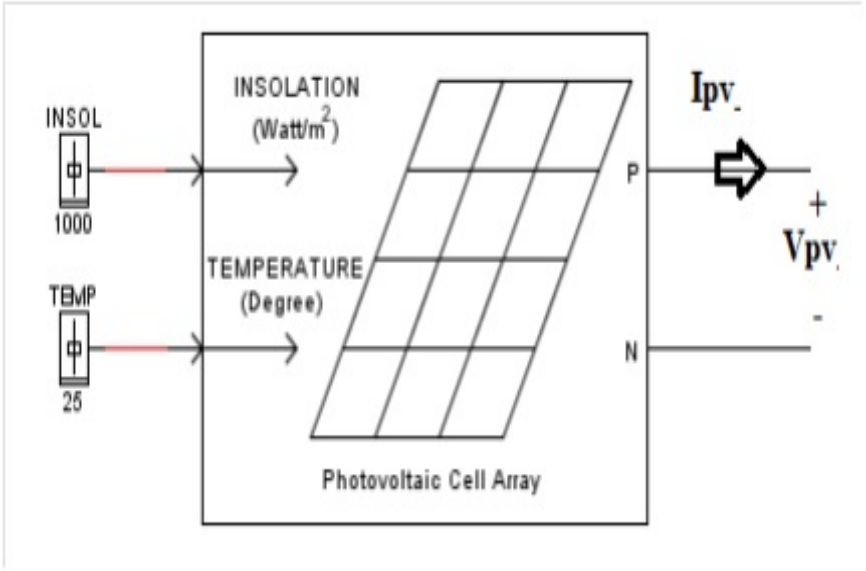

FIGURE 4.4: RTDS PV array model

4.2.1 Maximum Power Point Tracking(MPPT)

MPPT is the technique that is used by charge controllers to maximize the output of a PV system. The RTDS PV model performs the estimation of the maximum power point, for a particular solar insolation and temperature, using the following two analytical approximations:

1. Lambert Function approximation.

2. Fractional open circuit voltage approximation.

There are two ways to increase the output from the solar power. One of the ways is by increasing the number of solar panels. Another is by increasing the efficiency of the energy conversion in the system. In order to increase the efficiency of energy conversion, the energy being extracted from the solar cell needs to be increased.

4.2.2 Voltage Source Converter(VSC)

The conversion of the DC power generated by the PV system into AC power is done using a two level VSC. The conversion into AC power is necessary so that the system is properly integrated into the main grid. The switching elements, which are used in the converters are GTOs with anti-parallel diodes. The firing pulse to the GTO is generated by using a triangular wave, which acts as a modulating wave. The frequency of the triangular wave is adjusted according to the requirements. The solar system used is shown in Fig.(4.5)

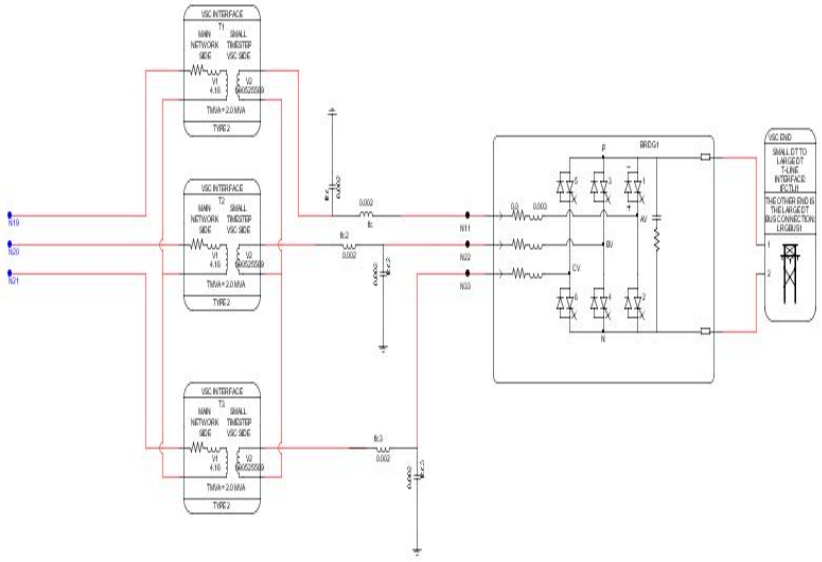

FIGURE 4.5: Solar Converter

4.3 High Impedance Fault Model

The various characteristics of HIF are non-linearity, low frequency of HIF currents and asymmetry. The model of HIF should be such that it contains all these characteristics. Many models have been proposed until now.

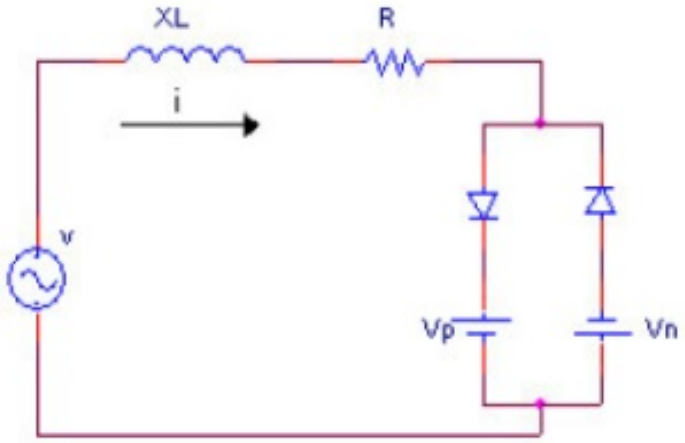

FIGURE 4.6: Enamuel Arc model of HIF

The enamuel arc model is shown in Fig.(4.6). This arc model for the simulation of HIFs was introduced in 1990. It is built on the basis of results from the laboratory experiments conducted, in order to better understand the phenomenon HIF. Then with the evolving understanding of the complex characteristics of HIFs, the model has been modified. But this basic model of HIF still retains its authenticity.

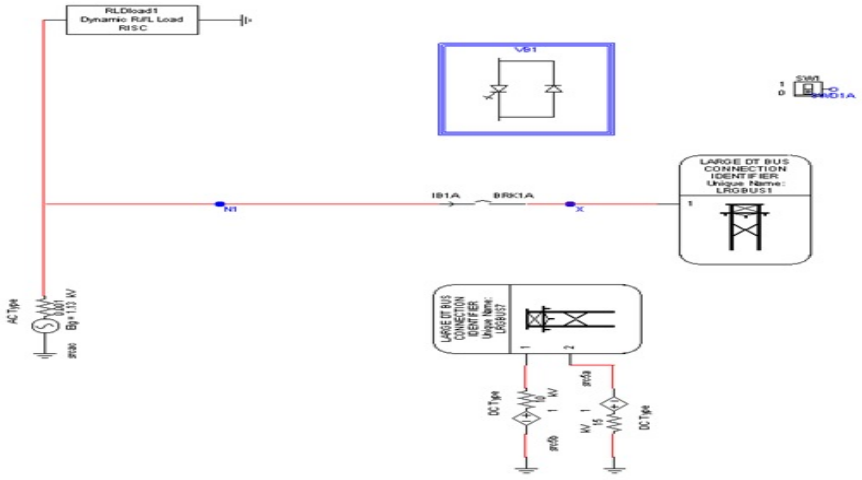

FIGURE 4.7: HIF model(large time step) in RTDS

The high impedance model simulated in RTDS is shown in Fig.(4.7) and Fig.(4.8). This fault model is based on the Emanuel model(shown in Fig.(4.6)) which was introduced

in 1990 [2].Emanuel model is based on laboratory measurements and theoretical components. The arc is modeled using two DC sources, connected as anti- paralleled by two diodes.

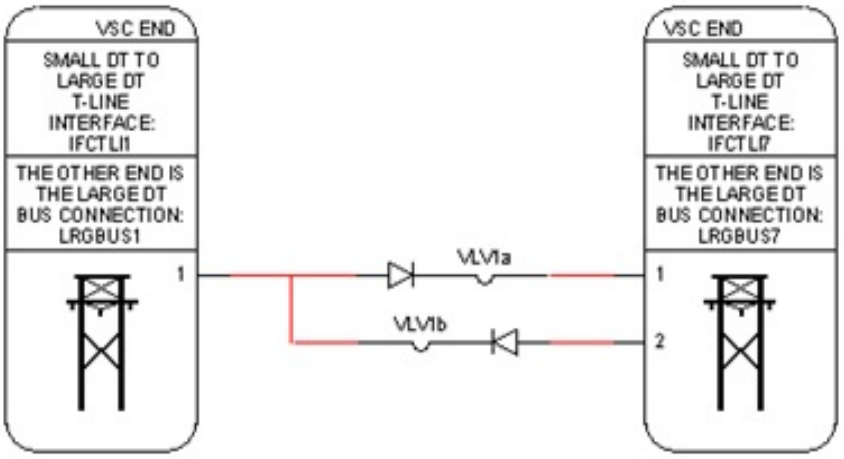

FIGURE 4.8: HIF model(small time step) in RTDS

The RTDS model consists of two dc sources with series resistances. There are two anti-parallel diodes. Since in RTDS the large time step and small time step components cannot be connected directly, therefore the diodes are kept in the hierarchy box are connected to the rest of the network through interface lines.

This model consists of only one arm. But in the main system this model consists of 4 to 5 arms connected to the system with different circuit breakers. These circuit breakers are fired alternatively. With different values of the dc sources and their series resistances and with different firing sequences of circuit breakers and varying time periods, different high impedance fault characteristics are generated.

4.4 5 bus system

Fig.(4.9) shows the schematic of the 5-bus system which is simulated in RTDS. There are two DGs used in this system. DG1 is the pv system and DG2 is wind system. There are two configurations for this system. C1 being the one in which the switch in line L5 is open and C2 being the one in which that switch is closed.

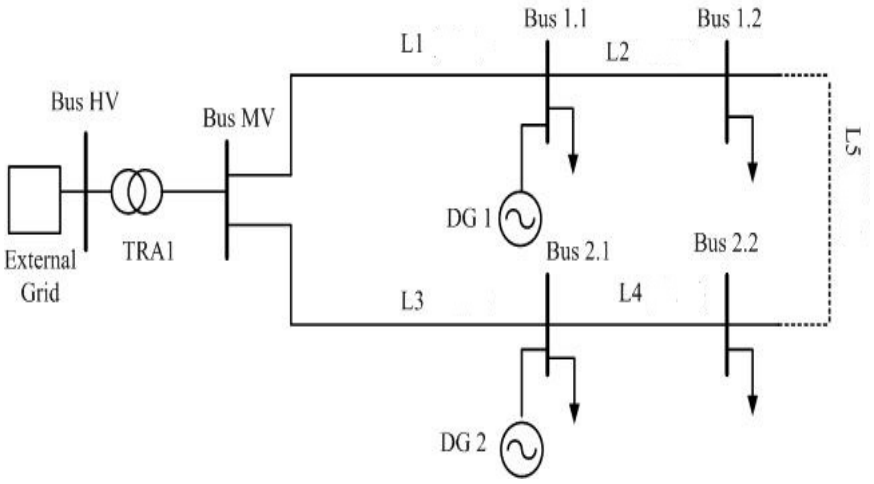

FIGURE 4.9: Single Line diagram of a 5-bus system

The capacity of the DGs used is 2 MW each. There are four loads connected at the four buses. When L5 is open, the system behaves as a normal radial system with DGs integrated and it becomes a ring structure when the line L5 is closed. For these two configurations, the optimal relay settings are determined.

Chapter 5

Detection Technique

This section consists of the techniques implemented for the detection of HIFs, islanding and optimizing the setting of a relay.

5.1 HIF fault detection technique

HIFs are very difficult to be detected by conventional overcurrent relays because of the fact that the fault current is very low. These faults occur when any high impedance object comes in contact with a primary distribution conductor and ground or when a conductor breaks and touches earth's surface like concrete, glass, asphalt, sand, sod etc. These surfaces offer very high impedances and the result is very low fault current. The two different fault detection techniques employed in this work are:

1. Fault detection based on estimation of harmonic components.
2. Fautl detetion using Mathematical Morphology.

5.1.1 Fault detection based on estimation of harmonic components

This technique utilizes the change of amplitude of the 3rd and 5th harmonic current components for the detection of HIF. Although 3rd harmonic current, alone, is sufficient for detection but the reason behind going for 5th harmonic current is that in some low

power converters, like the ones used in TV sets and battery chargers, 3rd harmonic components are very high. This can lead to false tripping.

Discrete Fourier Transform(DFT) technique is used to obtain the estimates of the 3rd and 5th harmonic components during normal operating condition and also during high impedance faults. It is observed that 3rd and 5th are the dominant harmonic components apart from the fundamental. The increase in the harmonic components is distinguishable as compared to the pre-fault values.

5.1.2 Fault detection using Mathematical Morphology(MM)

Mathematical morphology is a non-linear signal processing tool, in time domain, which transforms the shapes of the signals. The transformation is based upon integral geometry and set theory. The two elementary transformations in MM are dilation and erosion. There are a lot of other transformations which are derived from these two. The transformation task is performed by a signal processing function called Structuring Element(SE). The SE is selected on the basis of the type of application and this plays a very important role in MM operations. There are two more transformations which are used very frequently, namely opening and closing. They are also for one-dimensional signals. All these four transformations are now defined below:

The equation 5.1 defines the dilation of a signal.

$$y_d(n) = (f \oplus g)(n) = max\{f(n-m) + g(m)\}$$
$$0 \leq (n-m) \leq, m \geq 0 \tag{5.1}$$

Equation 5.2 defines the erosion of a signal.

$$y_e(n) = (f \ominus g)(n) = min\{f(n+m) - g(m)\}$$
$$0 \leq (n+m) \leq, m \geq 0 \tag{5.2}$$

Based on the above two elementary operations, we define the opening and closing operations in equations 5.3 and 5.4, respectively.

$$y_o(n) = (f \circ g) = (y_d \ominus g)(n) = ((f \ominus g) \oplus g)(n) \tag{5.3}$$

$$y_c(n) = (f.g)(n) = (y_d \ominus g)(n) = ((f \oplus g) \ominus g)(n) \tag{5.4}$$

The structuring elements serve as the basic building blocks of all the MM transformations and they are also used as probes tor extraction of feature. They can have different lenghts and they can acquire any shapes such as linear, sinusoidal, circular, square or any other geometrical shape. The major role in the selection of the structuring element is played by the frequency of interest and it is also application dependent. The choice of the SE is also influenced by some other factors like frequency spectrum, type of the signal and sampling rate. The most efficient choice will be the one which extracts the features of interest while suppressing other features. Eq.5.5 describes the Closing Opening Difference Operation(CODO). This operation is very effective for the detection of any disturbance in waveforms

$$y_{CODO}(n) = y_c(n) - y_o(n) = (f.g)(n) - (f \circ g)(n) \tag{5.5}$$

The first task is to detect the disturbance. A disturbance is said to be there if a spike occurs in the output of the CODO operation. The CODO value is calculated for every phase current and a threshold value is also set. The threshold value is set at 115% of the maximum CODO output during normal operation. Now the important task is to distinguish the HIF from other events which can cause disturbances. The HIF will generate a sequence of spikes which are distributed non-uniformally, distributed over a wide range of time. On the other hand, capacitor and load switching only generate either a single spike or there could be multiple spikes distributed over a short span of time, generally not longer than one-eighth of a cycle. The difference in the pattern of spikes is very clear. There does not occur any need for any learning based pattern recognition technique. Thus a rule based method is adopted.

The algorithm needs two more parameters- reset time(T_r) and wait time(T_w) for the successful detection of HIF. Wait time is required in order to avoid false tripping due to the initial multiple consecutive spikes which are generated by capacitor switching. After the completion of the wait time, algorithm waits for another spike in the CODO output. The occurrence of such a spike confirms the that this is due to an HIF. The extent to

which transients are present in the current waveform, determines the detection time or the detection delay for this second spike. Thus it becomes important to wait for even the spikes which are very widely separated. This wait time is termed as reset time. If during this reset time, no spike is detected then it is concluded that the disturbance encountered is not due to an HIF. But if a spike occurs between the wait time and the reset time, then the HIF flag is made high. If at the completion of the reset time, the HIF flag is high, a trip signal or an alarm will be generated, or else the algorithm is reset and is started again. Fig.5.1 shows the flowchart for the algorithm of detection of HIF by mathematical morphology.

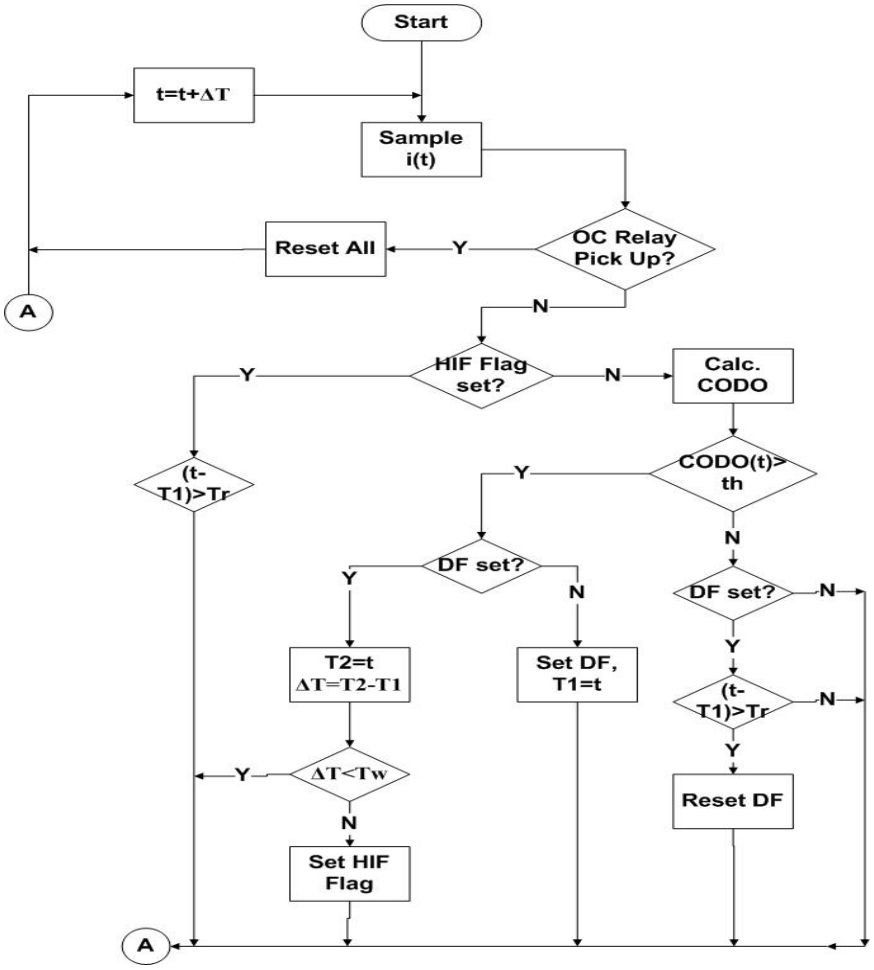

FIGURE 5.1: Flowchart for HIF detection method

5.1.3 Fault Direction Estimation

Once a fault is detected by a relay, the next step is to determine whether the fault is upstream of the relay or downstream. In this work a fault direction technique is proposed based on the calculation of the difference of the fundamental apparent power in both,

forward and reverse, cases. The fundamental apparent power is calculated by obtaining the product of the fundamental components of voltage and current. The fundamental components are obtained using discrete fourier transform(DFT). When a forward fault takes place, there is an increase in the apparent power seen by the relay. This is due to the increase in the fundamental component of the current. When a reverse fault takes place, there is a decrease in the apparent power seen by the relay. This property is exploited here to detect whether the fault has taken place upstream of the relay or downstream.

5.2 Islanding Detection

In this work, the product of change in positive sequence voltage and change in positive sequence current is used for islanding detection.

$$\Delta S_1 = \Delta V_1 * \Delta I_1 \tag{5.6}$$

The value of this parameter is calculated for different conditions. By varying the load, the mismatch between total amount of generated power and the total load is changed and for these values ΔS_1 is plotted against time.

The values of ΔV_1 and ΔI_1 are given as follows:

$$\Delta V_1 = abs(V_{post}) - V_{pre}) \tag{5.7}$$

$$\Delta I_1 = abs(I_{post} - I_{pre}) \tag{5.8}$$

where all these values on the right hand side are phasor quanties, computed by using DFT. The results obtained are then compared with some other events, like load switching and capacitor switching.

5.3 Optimal determination of the Relay Settings

The optimization of the relay settings is dependent upon the relay coordination for every possible network configuration, which is expressed as a non linear programming(NLP) optimization problem. The aim of the objective function is to minimize the total operating time of the primary and the backup relays, subject to the constraints imposed by the system operators.

The objective function is shown below:

$$minz_k = \sum_{f=1\forall(i,j)\epsilon P}^{N_F} \sum (t_{i,f}^k + t_{j,f}^k), k = 1, .., N_G \tag{5.9}$$

where the set P contains all the pairs of primary and backup relays. $t_{i,f}^k$ and $t_{j,f}^k$ being the response times, with confiuration k and at fault location f, of the primary and backup relays. N_F and N_G are the total number of fault locations considered and the available configurations.

$$t_{i,f}^k = TD_i^k * (\frac{A_k}{(I_{f,i}/I_{pu,i}^k)^{B_k} - 1} + C_k) \tag{5.10}$$

where A_k, B_k and C_k are constants. $TD_i^k, I_{pu,i}^k$ are the time dial settngs and the pickup current settings of the i^{th} relay in the k^{th} configuration. $I_{f,i}$ is the fault current seen be the i^{th} relay at location f. The other constraints to this optimization problem are

$$I_{pu,i}^{min} \leq I_{pu,i}^k \leq I_{pu,i}^{max}, i = 1, ..., N_R, k = 1, ..., N_G \tag{5.11}$$

$$TD_i^{min} \leq TD_i^k \leq TD_i^{max}, i = 1, ..., N_R, k = 1, ..., N_G \tag{5.12}$$

The constraint due to the coordination time interval(CTI) is

$$t_{j,f}^k - ti, f^k \geq CTI, \forall(i,j)\epsilon P, k = 1, ..., N_G, f = 1, ..., N_F \tag{5.13}$$

This optimization can be solved by the Particle Swarm Optimization(PSO).

5.3.1 Particale Swarm Optimization

PSO is inspired by the sociological behavior concerning flocking of birds and fish schooling. It does not require any kind of gradient information. This is the most attractive feature of PSO. This makes it usage possible even in those situations where it is not feasible to compute the gradient easily. In a PSO, there is a potential solution attached to every particle. A swarm is a cluster of all these particles. The particles are capable of remembering their present position. The objective function, velocity and the best position helps in finding the value of the current position of every particle in a swarm. The position of a particle which gives the best value of the objective function, is known as the personal best position(pbest) of that particle. In this work, where the objective is to minimize the objective function, the best value of the objective function is the one with the minimum value. In a swarm, the pbest of all the particles are compared and the best out of these is considered as the global best(gbest). During every iteration, the present velocity of every particle, its aloofness from the pbest and gbest helps in determining the new velocity of the particle.

$$V_i^{k+1} = V_i^k + c1 * rand() * \frac{pbest_i - s_i^k}{\delta t} + c2 * rand \frac{gbest_i - s_i^k}{\delta t} \tag{5.14}$$

where V_i^k is the velocity of the i^{th} particle during k^{th} iteration, s_i^k is the current position of the i_{th} particle, c1 and c being acceleration coefficients, $pbest_i$ and $gbest_i$ being the personal and global best positions of the i_{th} particle and δt being the time step.

Now every particle modifies its position according to the below equation,

$$s_i^{k+1} = s_i^k + v_i^{k+1} * \delta t \tag{5.15}$$

A modification is suggested to the velocity updating equation. This is done in order to accelerate the convergence.

$$V_i^{k+1} = \omega * V_i^k + c1 * rand() * \frac{pbest_i - s_i^k}{\delta t} + c2 * rand \frac{gbest_i - s_i^k}{\delta t} \tag{5.16}$$

where ω denotes the inertia weight. The inertia weight used is a linearly decreasing one, whose value decreases from 0.9 to 0.4.

The algorithm for the PSO is shown in Fig.5.2. The steps followed in the algorithm are as follows:

1. Initially random values are generated for the particles, which in this case are the time dial settings and plug settings of the various relays in that configuration.
2. With there initials values, the objective function is evaluated.
3. Now the value of the particle which gives the best results i.e. optimum value of the objective function, compared to the previous values of that particle is considered as the 'pbest' or personal best of that particle.
4. Of all these pbest values of the different particles in a swarm, the value which gives the optimum value of the objective function, which in this case is the minimum value of the objective function, is termed as the 'gbest' or global best value.
5. Using these pbest and gbest values and the current position of the particle, the velocity of the particle is updated.
6. A check for the maximum number of iterations is performed. If it is violated, then the solution obtained is the optimal solution otherwise it goes to step-2.

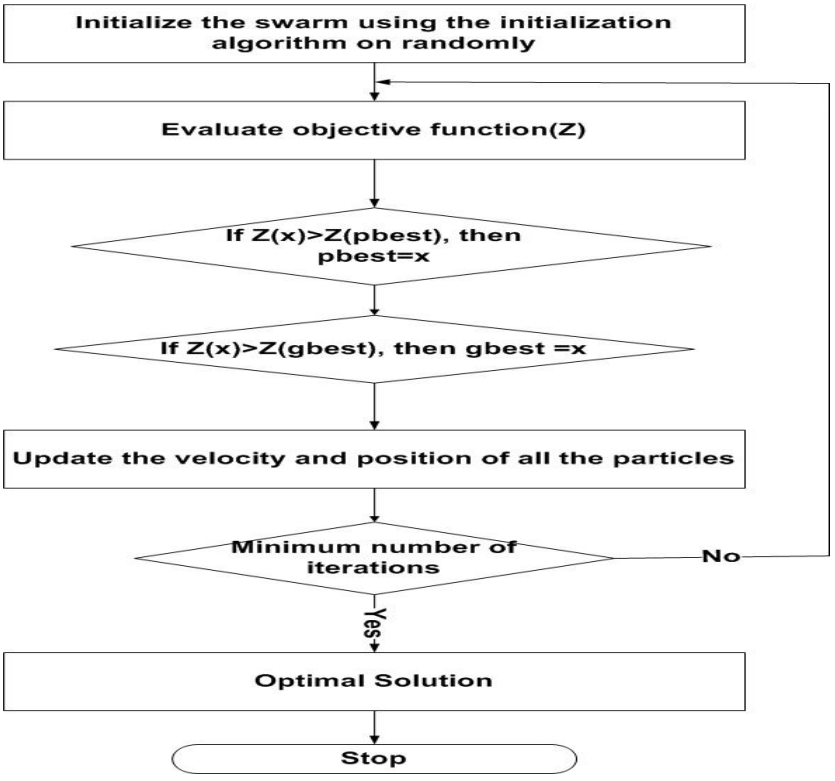

FIGURE 5.2: Flowchart of the PSO algorithm

Chapter 6

Results

This chapter shows the results for the different issues addressed in this work. Sec.6.1 shows the results of HIF detection for both the techniques used. Sec.6.2 shows the results for the islanding detection technique. The last section, Sec.6.3 shows the optimal relay settings obtained, for the negation of sympathetic tripping and protection system blinding.

6.1 HIF detection

High impedance fault occurs when a conductor gets broken and it touches ground or any other surface or when it comes in contact with a semi insulating surface. In this work both these faults are simulated and the results are shown.

This section shows the result for detection of high impedance faults using two techniques, namely:

1. By estimation of frequency components.
2. By mathematical morphology.

The results for HIF direction estimation are also shown. The direction of the HIF is estimated by observing the difference in the fundamental apparent power observed at the relay, near which the HIF occurs.

6.1.1 Fault detecton by estimation of frequency components

In this sub section the results for the detection of HIF, by using the frequency components present in the currents, are shown. The three different types of HIF characteristics are used for the simulation of HIF.

6.1.1.1 When the conductor touches a semi insulating object

Two different types of fault are created:

1. Between node 675 and the wind system.
2. Between node 671 and 684

The three different high impedance fault current characteristics simulated are shown in Fig. 6.1 (a) and (b) and Fig.6.2. These will be referred as type-1,2 and 3 respectively.

1. Fault current with intermediate characteristics

   This type of fault will be referred as type-1 fault in this section.

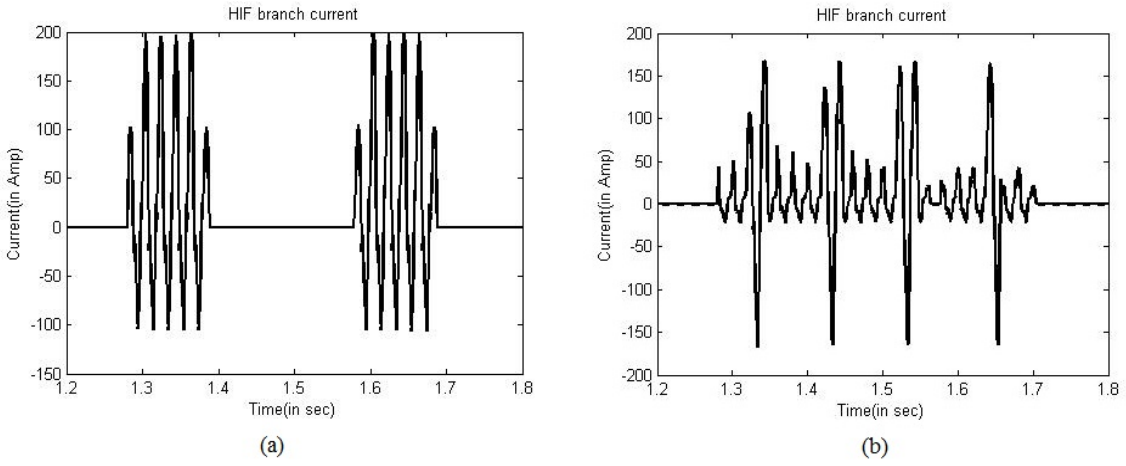

FIGURE 6.1: (a) Type-1 fault (b) Type-2 fault

This type of fault current characteristic is known as intermediate characteristics. This happens when a conductor comes in contact of some other surface for a short time moves apart. This can happen due to strong winds.

2. Fault current with spikes

   In this type of HIF, there are occasional spikes in current. Normally the current is of small magnitude but these high magnitude spikes occur randomly. This type of fault will be referred as type-2 fault in this section. The current waveform for type-2 fault is shown in Fig.6.1(b).

3. Type-3 Fault

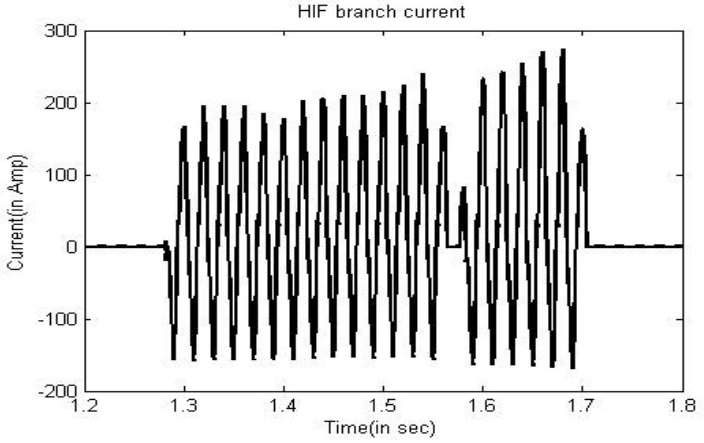

FIGURE 6.2: Type-3 HIF

   The results of these faults are then compared with capacitor switching and load switching.

The results of the harmonic estimation of the HIF current are now shown for the different types of HIF at different positions.

1. Fault between bus 675 and wind system

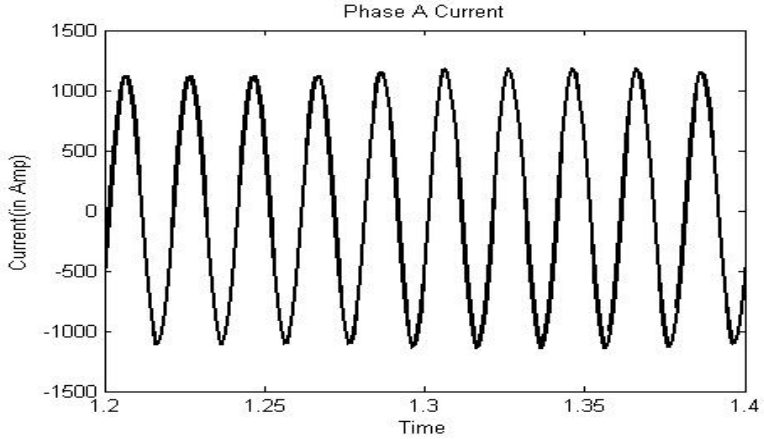

FIGURE 6.3: Phase A current for type-1 fault between bus 675 and wind system

Fig.6.3 shows the phase A current for a type-1 fault between bus 675 and the wind system. The fault is simulated in phase A in the middle of the line between bus 675 and the wind system.

The 3rd harmonic is the dominant one among the estimated harmonics in the point of view of the variation of magnitude. Its increasing magnitude for faulted phase is shown clearly in the Fig.6.4(a). Magnitude of 3rd harmonic component increases from a negligible pre fault value to close to 20A. For the healthy phases, the increase in magnitude is half of this value, 10 A approximately.

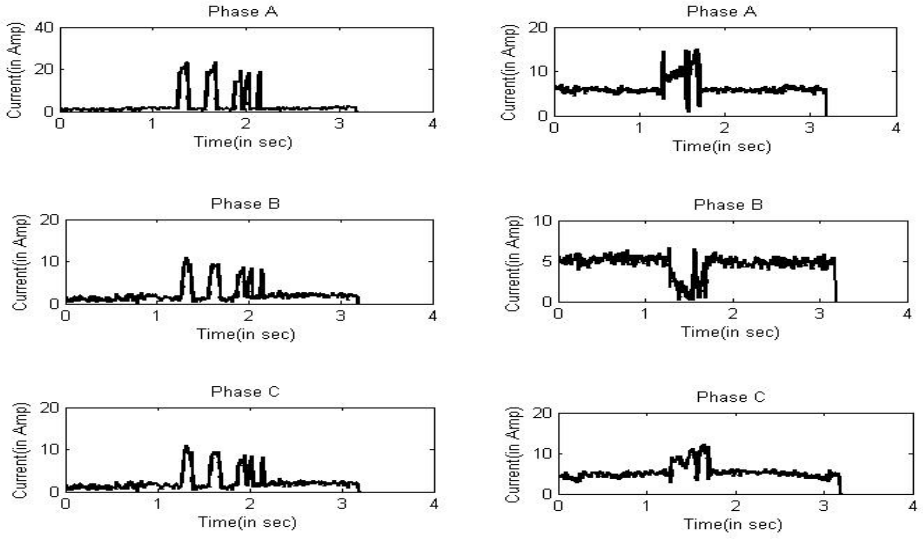

FIGURE 6.4: (a) 3rd and (b) 5th harmonic components for type-1 fault between bus 675 and wind system

The variation of 5th harmonic current component is shown in Fig.6.4(b). The 5th harmonic component in phase A increases from value of 8A to close to 20A. The increase in the healthy phases(B and C) is less. Although the variation is not as much as in 3rd harmonic, but it is sufficient in distinguishing between the faulted and the healthy phase.

Fig.6.5 shows the phase A current for a type-2 fault between bus 675 and the wind system. The slight increase in the current can be observed at 1.35 seconds.

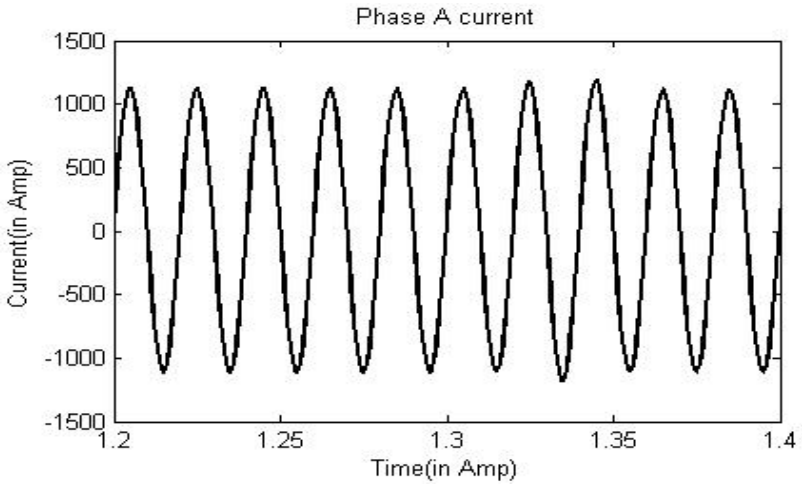

FIGURE 6.5: Phase A current for type-2 fault between bus 675 and wind system

From Fig.6.6(a) it can be observed that the increase in 3rd harmonic current component is highest in phase A, faulted phase, close to 20A while that of phase B and C is less, being around 8-9A in phase B and 5A in phase C. For 5th harmonic, the current increases from 8A to 18A in phase A. In phase B there is a decrease in current and in phase C, the increase in current is from 4A to 10A.

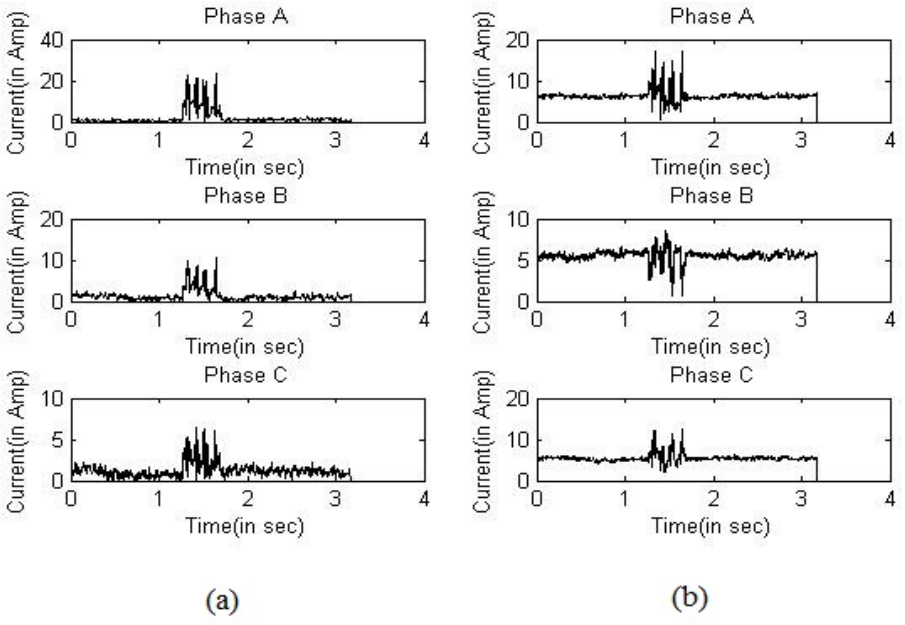

FIGURE 6.6: (a) 3rd and (b) 5th harmonic components for type-2 fault between bus 675 and wind system

The phase A current for a type-3 fault between bus 675 and the wind system is shown in Fig.6.7. At the point of fault, at 1.28 seconds, the current starts increasing, as was expected in this case. Increase in 3rd harmonic current for

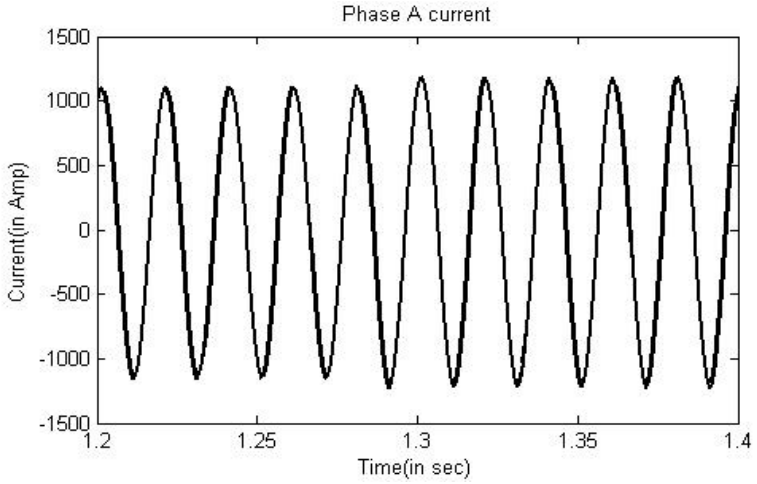

FIGURE 6.7: Phase A current for type 3 fault between bus 675 and wind system

phase A is from 0 to 20A and for phase B it is 0 to 10A. It is very small for phase C. 5th harmonic component increases from less than 10A to 18A in phase A. For phase B it decreases and increase in phase C current is limited to 10A.

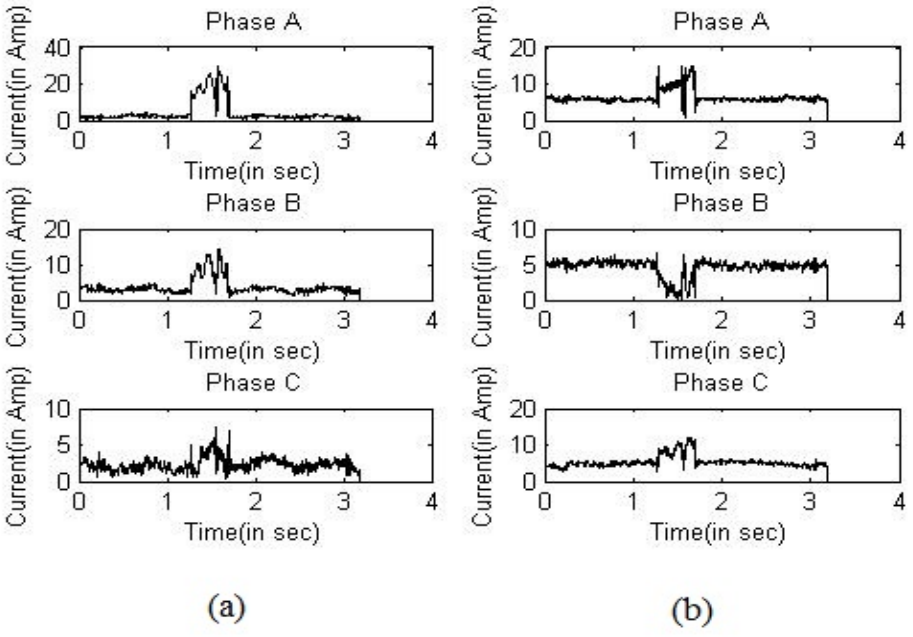

FIGURE 6.8: (a) 3rd and (b) 5th harmonic components for type-3 fault between bus 675 and wind system

From the above three fault cases, it can be concluded that the 3rd harmonic and 5th harmonic currents in the faulted phase increases a value of 15A, while for healthy phases this value is less. Thus 15A is taken as the threshold value for the relay for both 3rd and 5th harmonic.

2. Fault between bus 671 and 684

For the fault between bus 671 and 684, the current measurements are taken at bus 671.

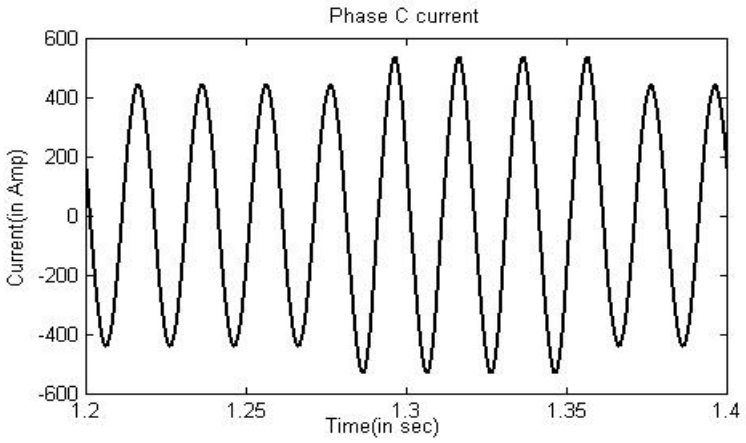

FIGURE 6.9: Phase C current for type-1 fault between bus 671 and 684

Fig.6.9 shows the phase C current when a high impedance fault takes place between bus 671 and 684 in phase C. Being an intermediate type of fault, there will be increase in current for a few cycles and no change in current for another few. This type of fault generally occurs when a conductor comes in contact with a semi-insulating surface for a few seconds and then gets awya from it. Due to this movement, there is increase in the value of the current.

Fig.6.10 shows the variation in the 3rd and 5th harmonic components for this type-fault, also known as intermediate type HIF. Increase in 3rd harmonic current for both phase A and B is less than 1A. It is close to 20A for phase C. Considering 5th harmonic current component, it can be seen that there is decrease in phase A current and a less than 1A increase in phase A. For phase C the increase is from 2A to 9A.

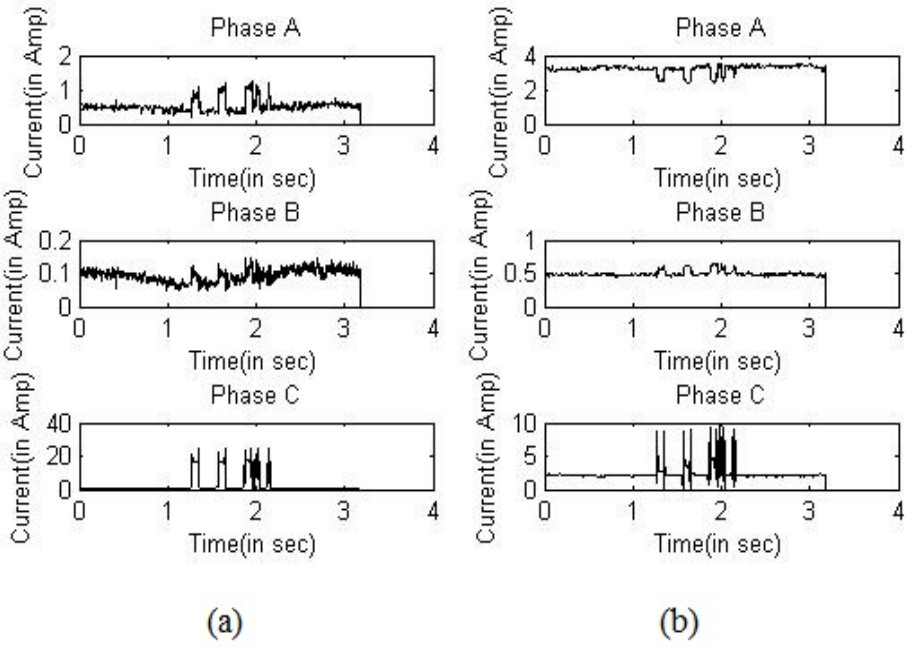

FIGURE 6.10: (a) 3rd and (b) 5th harmonic components for type-1 fault between bus 671 and 684

Phase C current for type 2 fault between bus 671 and 684 is shown in Fig.6.11. This type of fault causes random spikes in the phase current, due to which it is also known as the spikes type HIF.

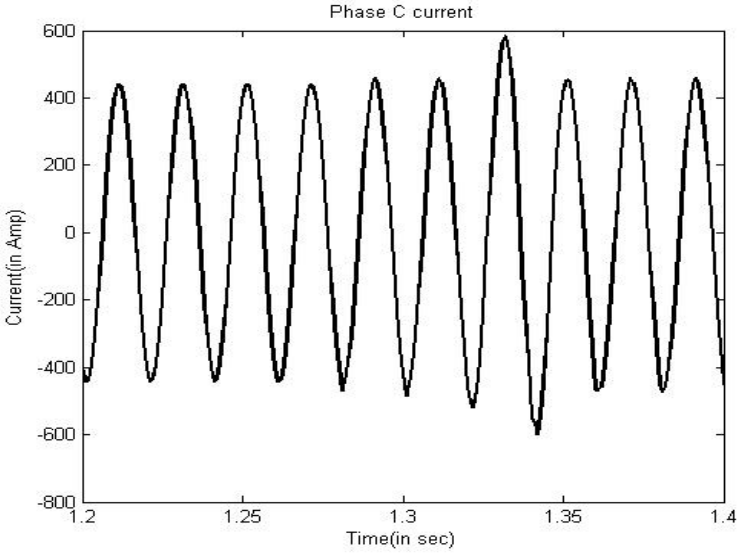

FIGURE 6.11: Phase C current for type-2 fault between bus 671 and 684

In both phase A and B, the increase in 3rd and 5th harmonic current is less than 1A, while it being more than 30A for phase C. For 5th harmonic, phase A and B

current are more or less constant. Phase C current increases from a value of 0A to 20A.

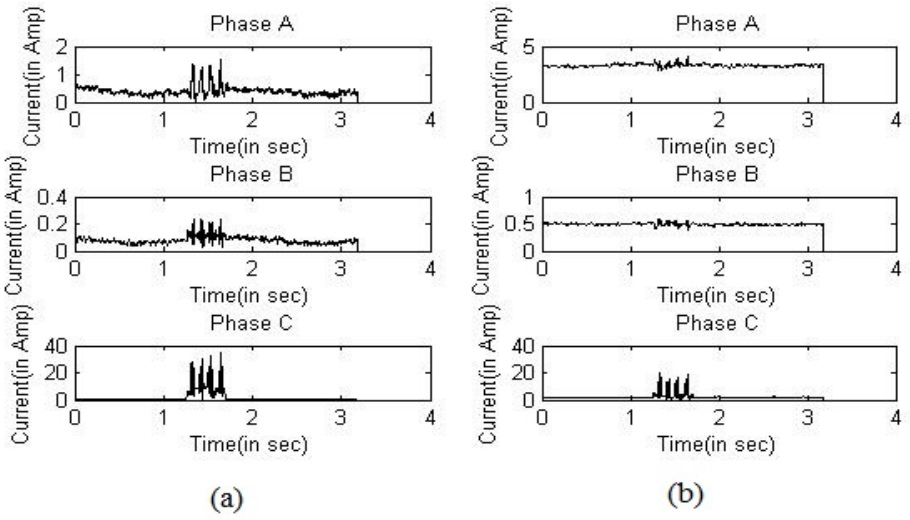

FIGURE 6.12: (a) 3rd and (b) 5th harmonic components for type-2 fault between bus 671 and 684

Phase C current for type 3 fault between bus 671 and 684 is shown in Fig.6.13.

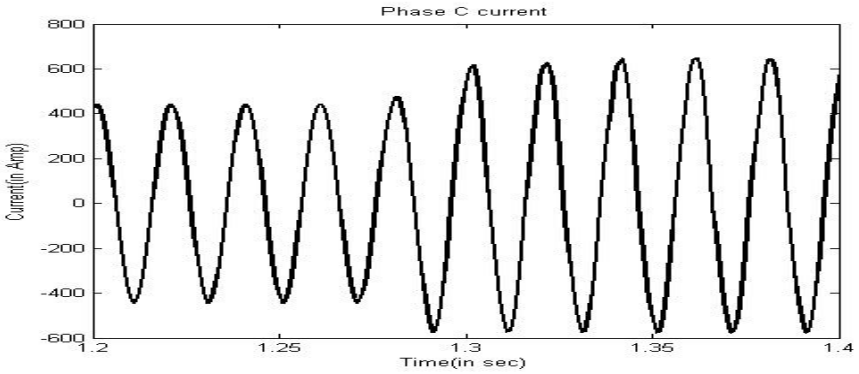

FIGURE 6.13: Phase C current for type-3 fault between bus 671 and 684

For phase A, 3rd harmonic current increases to 2A and 5th harmonic current is almost constant. For phase B, the increase in 3rd harmonic current is less than 1A and 5th harmonic current is almost constant. For phase C, 3rd harmonic increases from 0A to more than 40A and 5th harmonic changes from 3A to 18A.

Thus the threshold value for the relay at bus 671 is taken as 10A for 3rd harmonic and 5A for 5th harmonic.

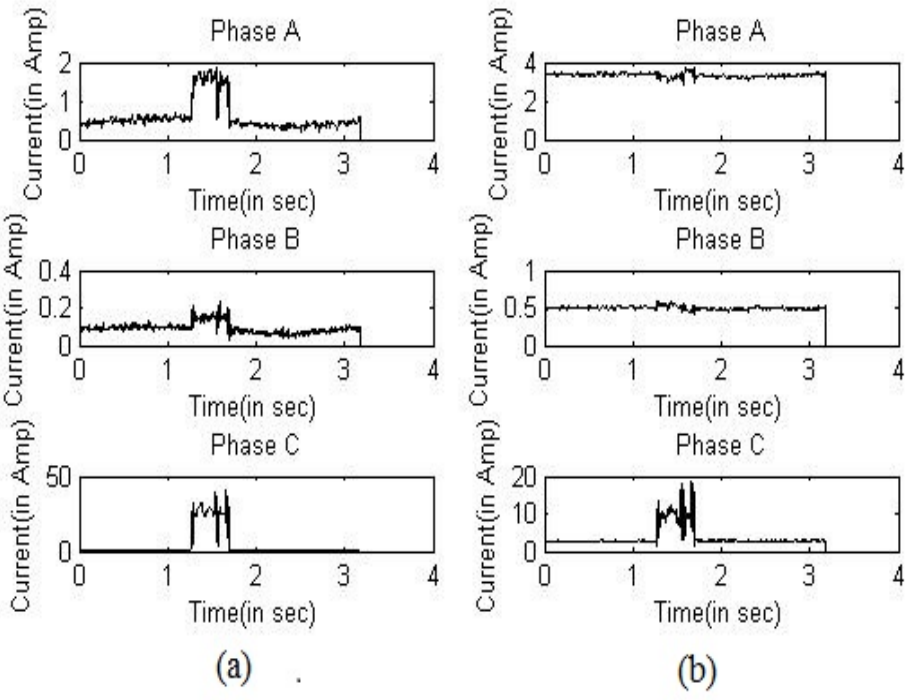

FIGURE 6.14: (a) 3rd and (b) 5th harmonic components for type-3 fault between bus 671 and 684

6.1.1.2 When the conductor falls on the ground(Case-2)

Fig.6.15 shows the line current for this case. This type of fault occurs when the conductor gets broken and falls on the ground(sand, clay or any other surface). There is no load current in the line, once the fault takes place.

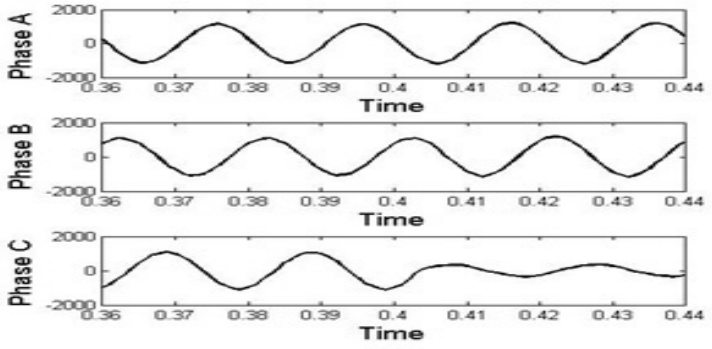

FIGURE 6.15: Line Current for HIF in phase C for case-2

Fig.6.16(a) shows the third harmonic current magnitude in all the phases. It can be seen from this plot that the increase in third harmonic current component in phase A and B, i.e. healthy phases, is around 20 A. While that in phase C, faulted phase, is around

100A. Thus there is a large increase in the third harmonic current in a faulted phase when compared to the healthy phases.

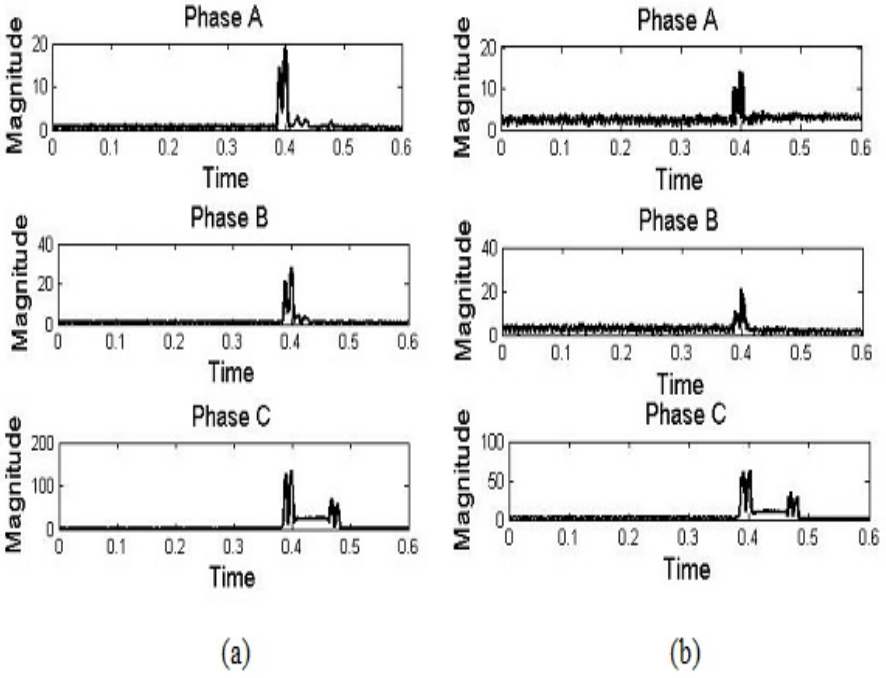

FIGURE 6.16: (a) 3rd and (b) 5th harmonic components for type-3 fault between bus 632 and 671(Case-2)

Fig.6.16(b) shows the fifth harmonic current magnitude in all the three phases. It can be seen from this plot that the increase in fifth harmonic current component in phase A and B, i.e. healthy phases, is around 10A and 20 A respectively. While that in phase C, faulted phase, is around 50A. Therefore there is a large increase in the fifth harmonic current in a faulted phase when compared to the healthy phases.

Therefore with a large increase in both the 3rd and the 5th harmonic current components we can conclude that the fault is in phase C. The threshold for the fault is set at 50A for 3rd harmonic and 40A for 5th harmonic.

6.1.1.3 Capacitor Switching

In this case, a 3 phase capacitor bank located at bus 675 and single phase capacitor located at bus 611 is switched in and out. The current is measured at both the buses. 3rd and 5th harmonic components are obtained by DFT method and their magnitude is analyzed.

From Fig.6.17(a) and (b), it is observed that when a three phase capacitor bank is taken out, there occurs a decrease in both the 3rd and 5th harmonic components. This change is small. It can be seen that it is clearly different from the harmonic variations obtained during a HIF.

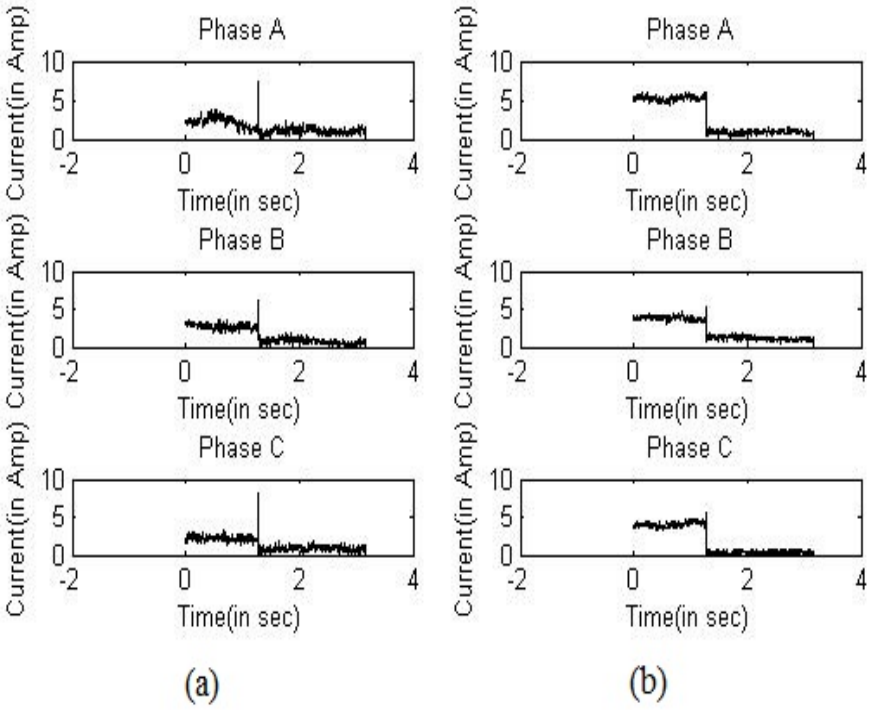

FIGURE 6.17: (a) 3rd and (b) 5th harmonic components when 3 phase capacitor is switched out

From Fig.6.18(a) and (b), it is observed that when a three phase capacitor bank is switched in, there occurs a increase in both the 3rd and 5th harmonic components. There is a spike initially but the overall change is small. It can be seen that it is clearly different from the harmonic variations obtained during a HIF.

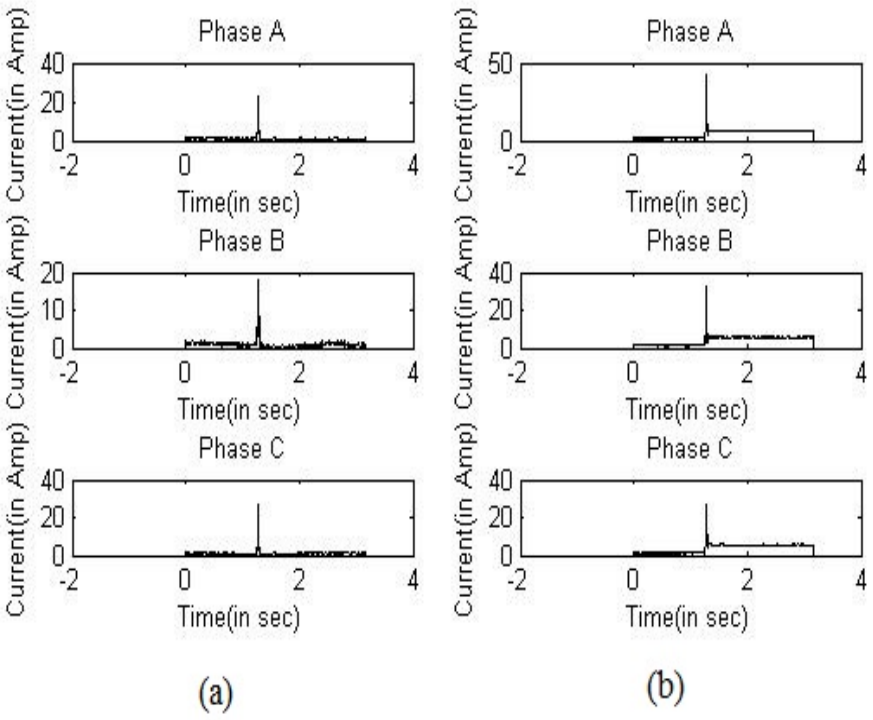

FIGURE 6.18: (a) 3rd and (b) 5th harmonic components when 3 phase capacitor is switched in

A single phase capacitor is located at bus 611. The currents measurements during capacitor switching are taken at bus 648. Capacitor is in phase C at the bus 611.

Fig.6.19 below shows the variation of the 3rd harmonic and 5th harmonic current components of phase C at bus 678 during capacitor switching.

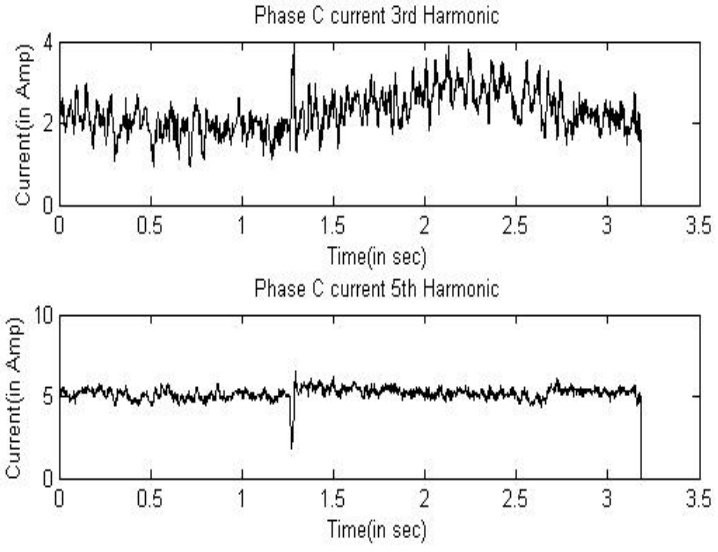

FIGURE 6.19: (a) 3rd and (b) 5th harmonic components when a single phase capacitor is switched in

The 3rd and 5th harmonic variations when the capacitor is switched in are negligible. When the capacitor is taken out, there occurs a spike in current components but it is for a very small period.

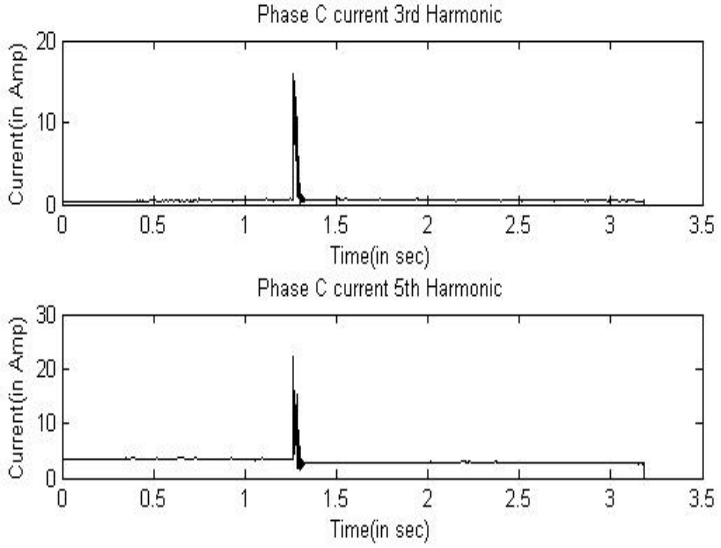

FIGURE 6.20: (a) 3rd and (b) 5th harmonic components when a single phase capacitor is switched out

6.1.1.4 Load Switching

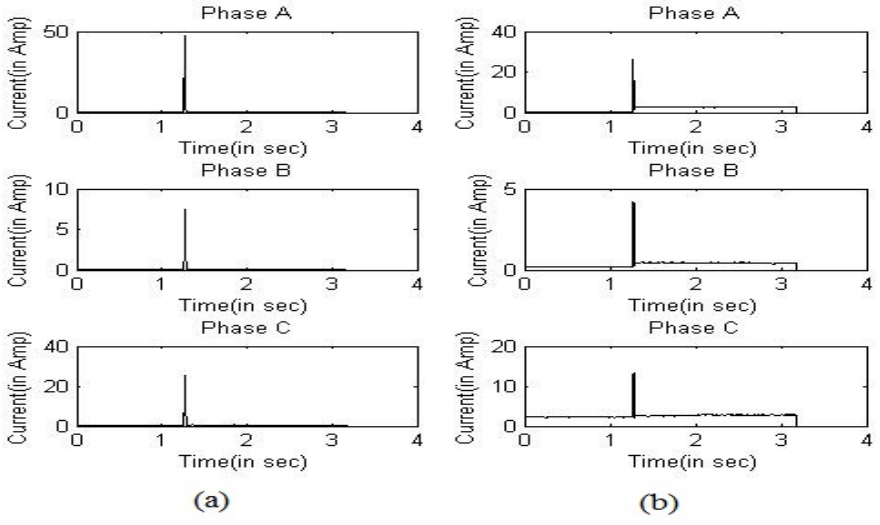

FIGURE 6.21: (a) 3rd and (b) 5th harmonic components when a load at bus 652 is switched in

In this case, loads at bus 675 and 652 are switched in and out. Both the loads are balanced loads. The current measurements are taken at bus 675 and 671 respectively.

3rd and 5th harmonic components are obtained by DFT method and their magnitude is analyzed.

From Fig.6.21(a) and (b) it is observed that when a 3 phase load is switched in, then there is spike at the instant of switching. Apart from that there is very slight change in the magnitude of harmonic components. Thus it is easily distinguishable from HIF.

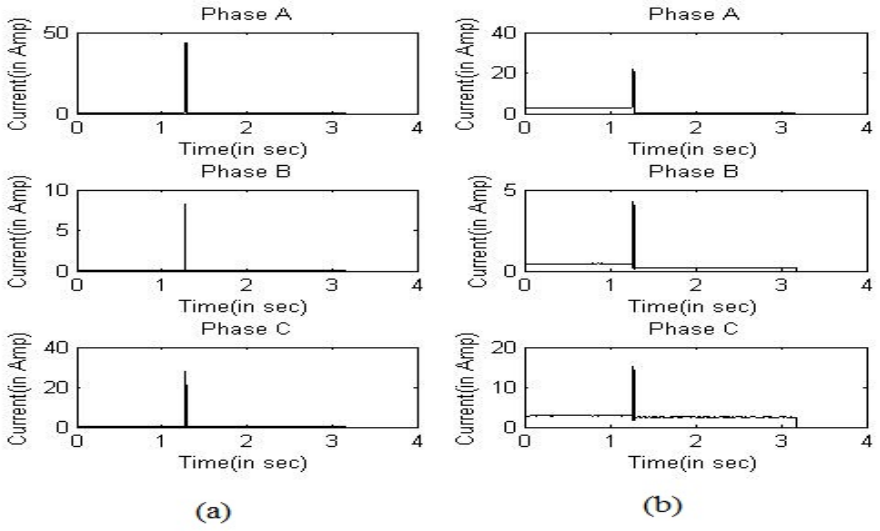

FIGURE 6.22: (a) 3rd and (b) 5th harmonic components when a load at bus 652 is switched out

Similar to the case of load switching in, there is also a spike when the load is taken out. Same conclusion can be drawn from this case also.

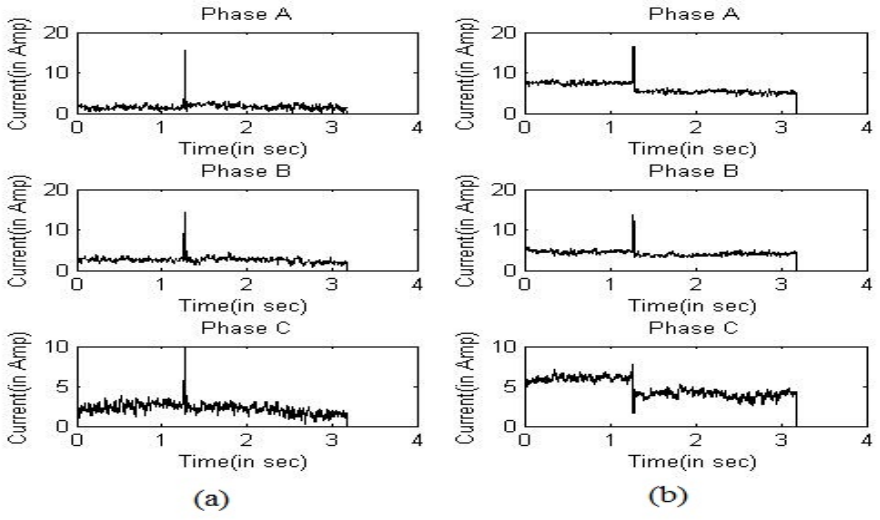

FIGURE 6.23: (a) 3rd and (b) 5th harmonic components when a load at bus 675 is switched in

Fig.6.23(a) and (b) shows the variation of the 3rd and 5th harmonic current components when load at bus 675 is switched in. Similarly Fig6.24(a) and (b) shows the same variation when the load at bus 675 is switched out. Thus from these two figures, it can be concluded that for the case of load switching, there occurs a spike in current for a very short time period and thus it can be distinguished from the HIF.

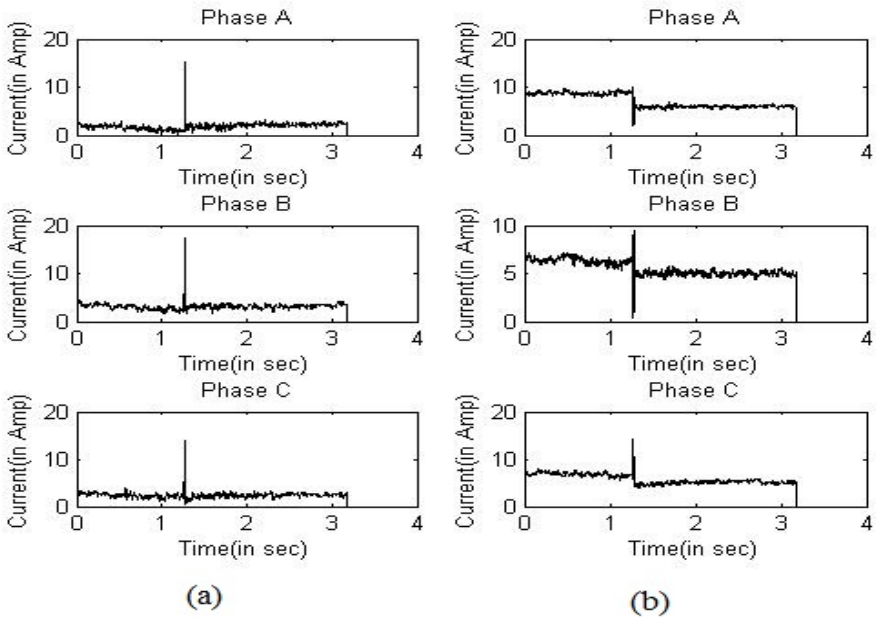

FIGURE 6.24: (a) 3rd and (b) 5th harmonic components when a load at bus 675 is switched out

6.1.2 HIF detection by Mathematical Morphology

6.1.2.1 Type-1 fault between bus 675 and wind system

The wait time is taken to be of 1 cycle of the fundamental signal i.e. 20ms and the reset time is taken to be 0.5s.

Fig.6.25 shows the opening and closing operation on the normalized current. It can be observed that the output of the operations is almost same, due to which the value of CODO is quite small. The threshold value for CODO is taken as 1.15 times the maximum prefault value. In this case, it is 0.0002875. It can be seen from the waveform of CODO that the spikes, higher than the threshold, are large in number, which are indicative of the high impedance fault.

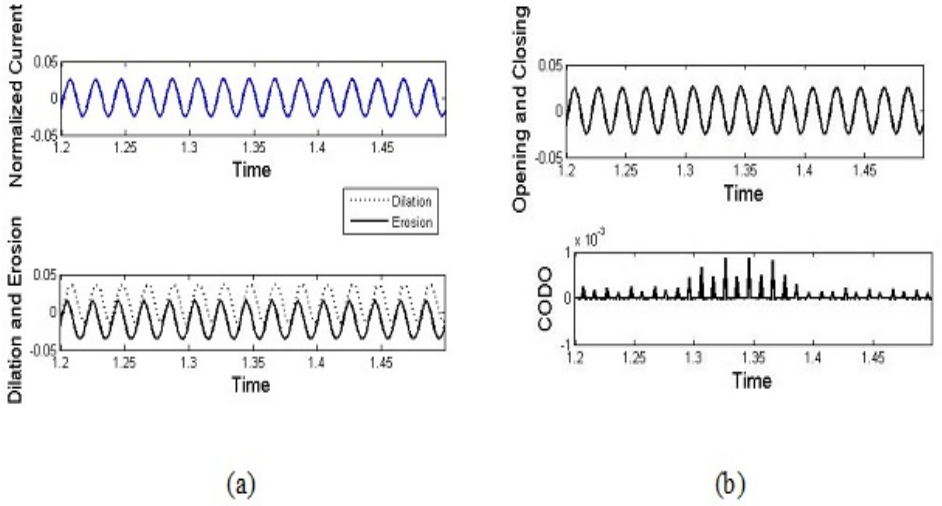

FIGURE 6.25: (a) Normalized current and dilation/erosion (b) Opening/closing and CODO for type-1 fault between bus 675 and wind system

Maximum CODO values for:

Prefault- 0.00025

Postfault- 0.00091

6.1.2.2 Type-1 fault between bus 632 and 645

Fig.6.26 shows the opening and closing operation on the normalized current.

Maximum CODO values for:

Prefault- 0.0012

Postfault- 0.0022

The threshold value for the CODO is set at 0.00138. The threshold value for CODO is set at 1.15 times the prefault value, as was done in the previous case. In this case also, it can be seen from the waveform of CODO that the spikes, higher than the threshold, are large in number, which are indicative of the high impedance fault.

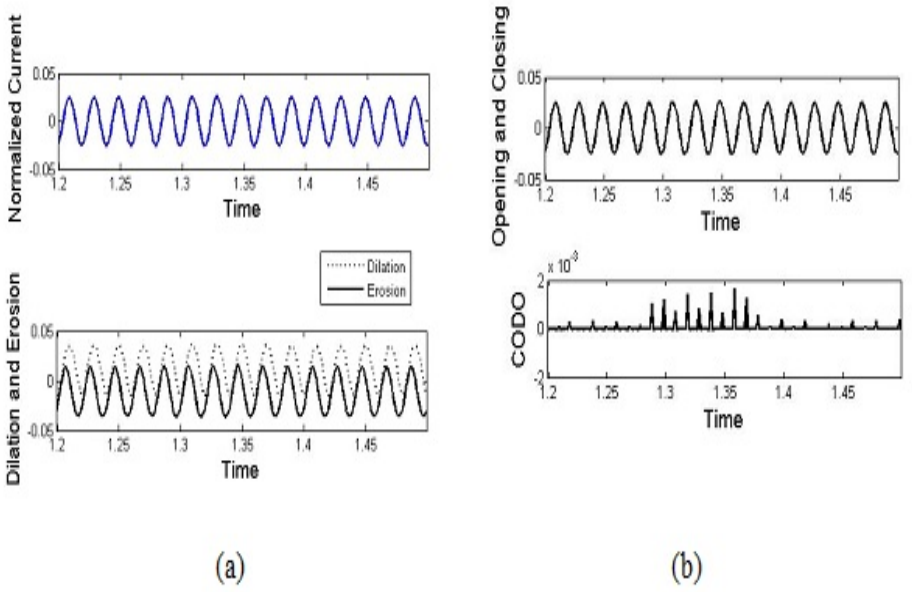

FIGURE 6.26: (a) Normalized current and dilation/erosion (b) Opening/closing and CODO for type-1 fault between bus 632 and 645

6.1.2.3 Type-2 fault between bus 632 and 645

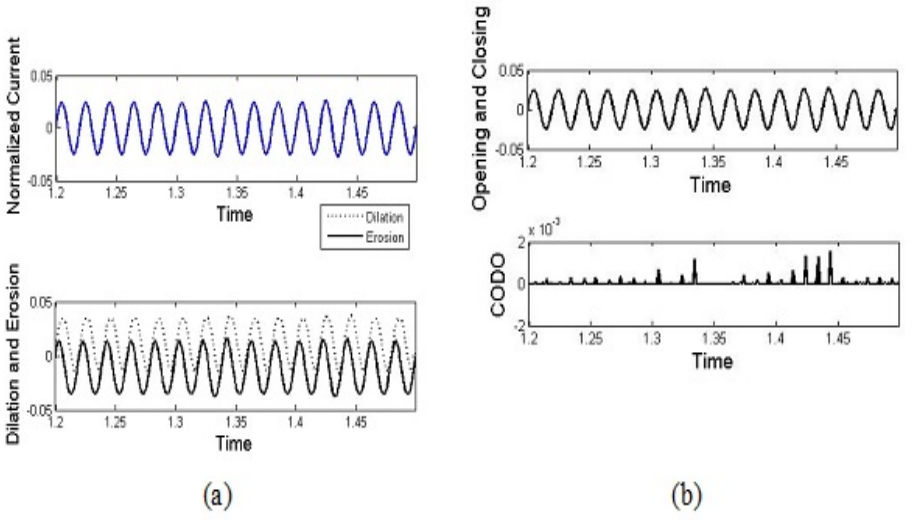

FIGURE 6.27: (a) Normalized current and dilation/erosion (b) Opening/closing and CODO for type-2 fault between bus 632 and 645

Maximum CODO values for:

Prefault- 0.0011

Postfault- 0.0015

The threshold value is set at 0.001265. The CODO output is shown in Fig.6.27(b), In this case also, it can be seen from the waveform of CODO that the spikes, higher than the threshold, are large in number, which are indicative of the high impedance fault.

6.1.2.4 Type-3 fault between bus 671 and 684

Maximum CODO values for:

Prefault- 0.0015

Postfault- 0.0041

Threshold value for this case is taken as 0.001725. . It can be seen from the waveform of CODO in Fig.6.28 that the spikes, higher than the threshold, are large in number, which are indicative of high impedance fault.

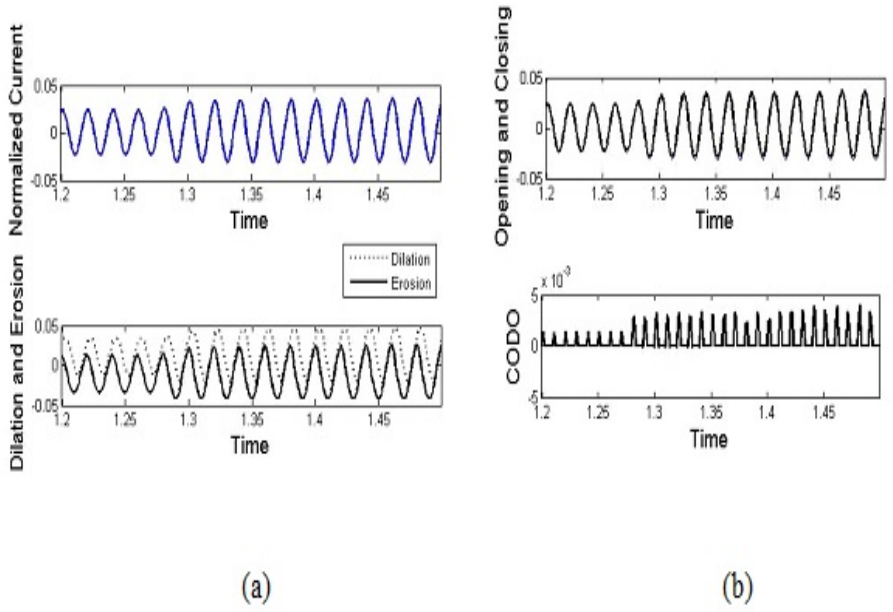

FIGURE 6.28: (a) Normalized current and dilation/erosion (b) Opening/closing and CODO for type-3 fault between bus 671 and 684

6.1.2.5 Capacitor Switching

Fig.6.29 shows the CODO for 3 phase capacitor switching. From the figure, it can be observed that there are no multiple spikes, as in the case of high impedance fault. Thus this property can be exploited to distinguish from a high impedance fault.

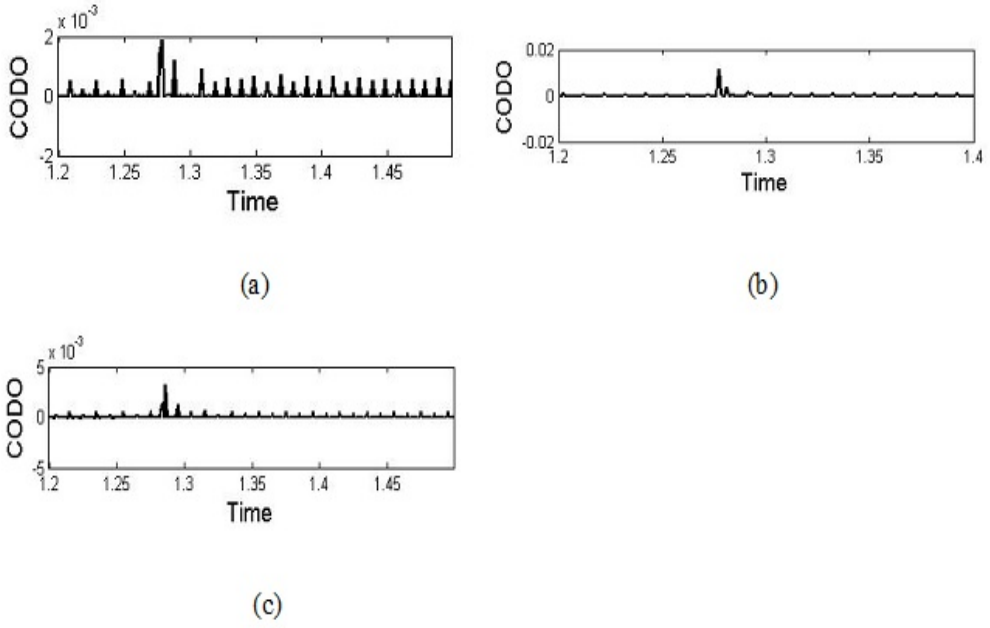

FIGURE 6.29: (a) Phase A (b) Phase B (c) Phase C CODO outputs for 3 phase capacitor switching

Fig.6.30 shows the CODO output for single phase capacitor switching in phase B. Similar observations, as in the case of 3 phase capacitor switching, can be made here to distinguish this condition from a high impedance fault.

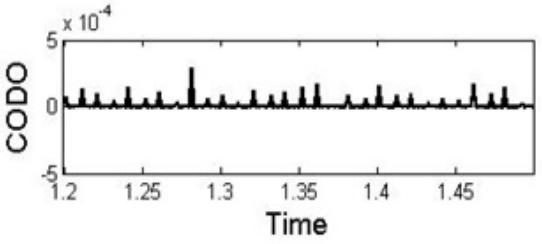

FIGURE 6.30: CODO output for phase B for single phase capacitor switching

6.1.3 Fault Direction Estimation

Once a high impedance fault is detected by a relay, the next task is to determine the direction of fault. Whether it is in forward direction or in reverse direction. Here different types of HIF are generated in the both the forward and backward direction of the relays at different locations.

6.1.3.1 Type-1 HIF for the relay placed at bus 675

Here a high impedance fault was simulated in forward and reverse direction of the relay placed at bus 675. The results are shown in Fig.6.31. The difference comes out to be positive for a forward fault and negative for a reverse fault. This characteristic is exploited for the estimation of the direction of an HIF.

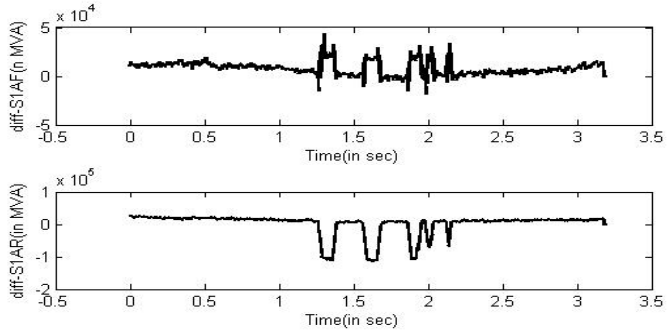

FIGURE 6.31: Apparent Power difference for forward and reverse type-1 fault for relay at bus 675

6.1.3.2 Type-1 HIF for the relay placed at bus 632

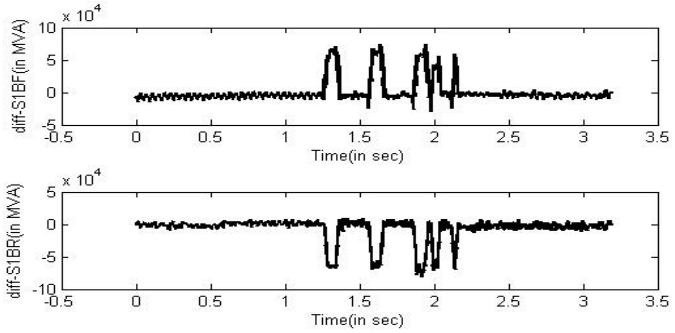

FIGURE 6.32: Apparent Power difference for forward and reverse type-1 fault for relay at bus 632

The high impedance fault was simulated in forward and reverse direction of the relay placed at bus 632. The waveform of the difference in the apparent power is shown in Fig.6.32. Again the results are as expected. For a fault in the forward direction, the difference comes out to be positive, while it is negative for the fault in the reverse direction.

6.1.3.3 Type-2 HIF for the relay placed at bus 675

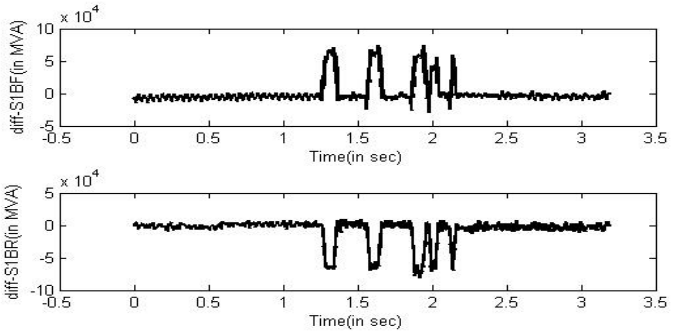

FIGURE 6.33: Apparent Power difference for forward and reverse type-2 fault for relay at bus 675

In this case, a type-2 high impedance fault was simulated in forward and reverse direction of the relay placed at bus 675. Type-2 indicates the HIF current with spikes. The results are shown in Fig.6.33.

6.1.3.4 Type-3 HIF for the relay placed at bus 675

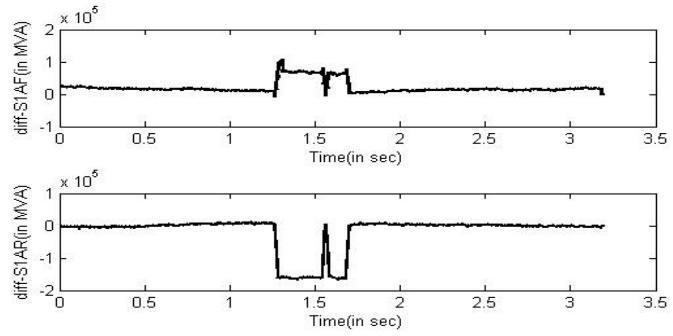

FIGURE 6.34: Apparent Power difference for forward and reverse type-3 fault for relay at bus 675

The high impedance fault of type-3 was simulated in forward and reverse direction of the relay placed at bus 675. The waveforms for the difference in apparent power are shown in Fig.6.34.

6.1.3.5 Type-3 HIF for the relay placed at bus 632

The high impedance fault was simulated in forward and reverse direction of the relay placed at bus 632. The results are shown in Fig.6.35.

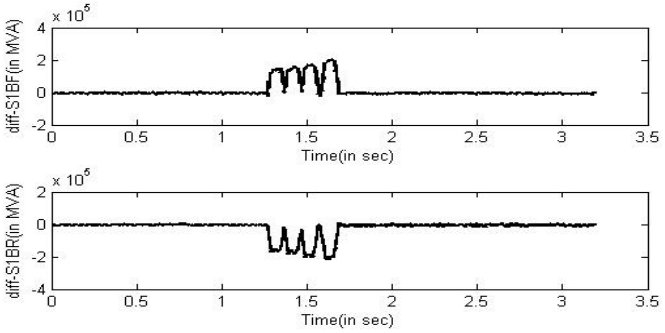

FIGURE 6.35: Apparent Power difference for forward and reverse type-3 fault for relay at bus 675

It can be inferred from all these results that when a forward high impedance fault takes place at a relay, there is an increase in the fundamental apparent power seen by the relay. And during a reverse fault there is a decrease in the apparent power. This technique can be used to detect the direction of fault at a relay.

6.2 Islanding Detection

In this section, the results for the islanding detection technique are shown. The product of change in positive sequence voltage and current is observed. Absolute values of this change in voltage and current are taken. The voltage and current are the phasor quantities, which are obtained after taking the DFT of these values. This parameter(product) is used to distinguish it from other events such as capacitor switching and load switching. So this section shows the results for the case of islanding, with different percent of real and reactive power mismatch, and also for the case of capacitor and load switching.

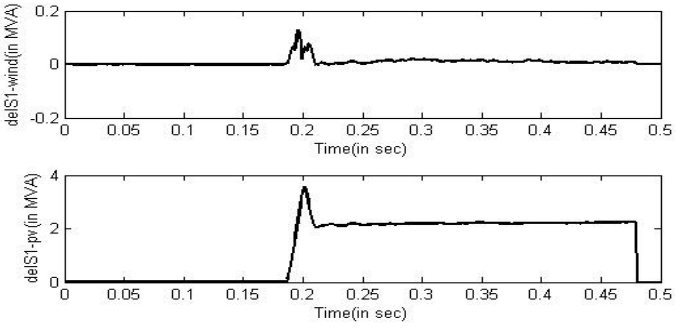

FIGURE 6.36: Positive sequence apparent power difference(in MVA) for a 10% real power mismatch

Fig.6.36 shows product of the difference in the positive sequence quantities when there is an islanding event, considering a 10% mismatch between load and generation. In this

case, a positive mismatch i.e. when the total load is 10% more than the total generation is considered. The results for the negative mismatch will also be the same. Thus here only the waveforms for positive mismatch are shown. The total load in the system in this case is 4.4MW.

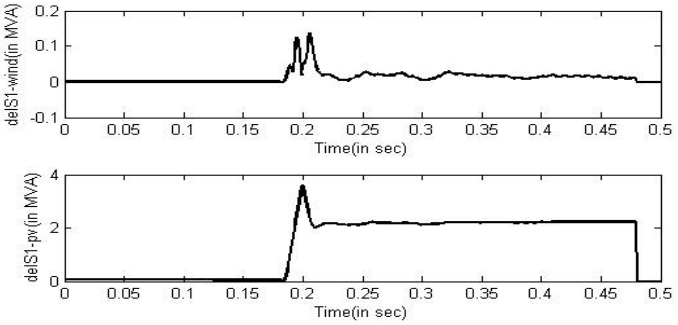

FIGURE 6.37: Positive sequence apparent power difference(in MVA) for 20% real power mismatch

Fig.6.37 and Fig.6.38 shows the difference in the apparent power due to the positive sequence components, given 20% and 30% mismatch between real power generation and load. The total generation capacities of the DGs are 4 MW. In these two cases, the total load in the system is 4.8MW and 5.2MW. In both the cases, the total increase near the bus, to which the wind generator is connected is around 0.15 MVA, while it is 3.5 MVA for the bus near PV system.

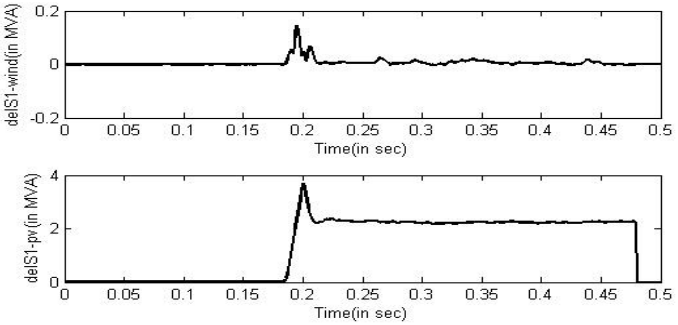

FIGURE 6.38: Positive sequence apparent power difference(in MVA) for 30% real power mismatch

Till now the waveforms in Fig.6.36, 6.37 and 6.38 were showing the results for islanding operation in case of real power mismatch. The next three figures will be showing the results in case of reactive power mismatch.

Fig.6.39 shows the resuls for a 10% reactive power mismatch between generation and load. The change in the positive sequence apparent power is around 0.1 MVA for the wind generator bus, while it is close to 3.5 MVA at the bus near the pv system.

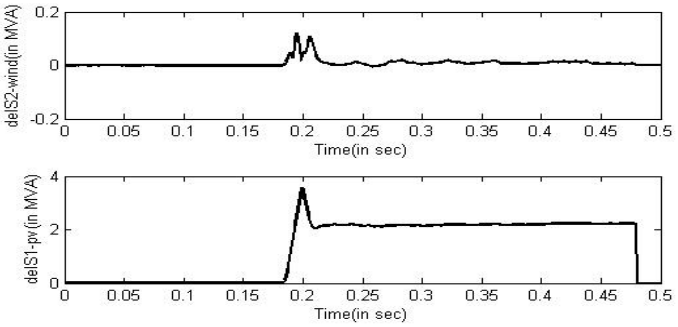

FIGURE 6.39: Positive sequence apparent power difference(in MVA) for 10% reactive power mismatch

Fig.6.40 shows the power difference for the case of 20% reactive power mismatch. In this case, as it can be observed from the figure, the change is around 0.1 MVA for wind generator bus and it is 3.5 KVA for the pv system bus.

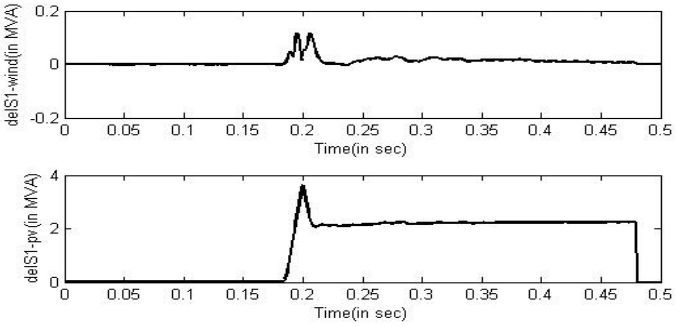

FIGURE 6.40: Positive sequence apparent power difference(in MVA) for 20% reactive power mismatch

Fig.6.41 shows that the change in the positive sequence apparent power is around 0.1 MVA for the bus near the wind system and its 3.5 KVA for the one near the pv system.

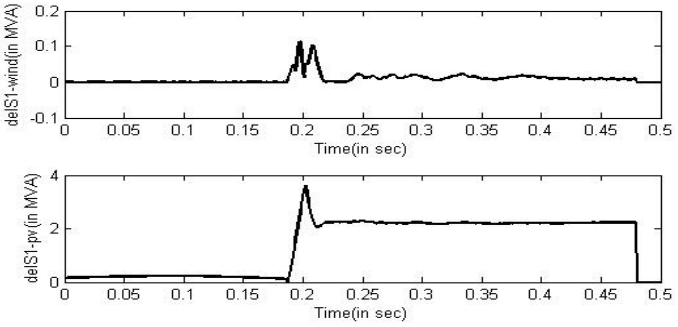

FIGURE 6.41: Positive sequence apparent power difference(in MVA) for 30% reactive power mismatch

All the results shown till now for both the real and reactive power mismatch indicate that when the islanding operation takes place, there is a change in the apparent power, that is being observed. This change can be a useful parameter in determining whether an islanding operation has taken place or not.

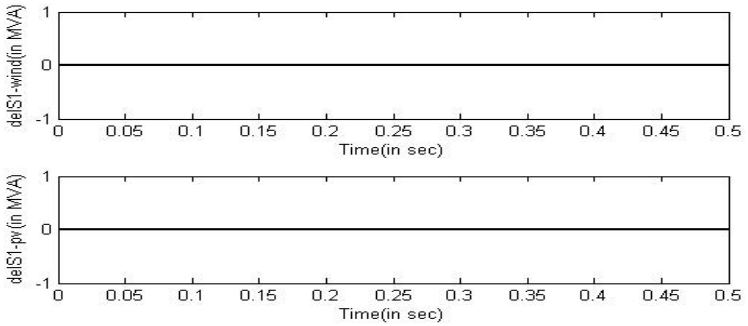

FIGURE 6.42: Positive sequence apparent power difference(in MVA) for capacitor switching

Fig.6.42 shows the waveforms when a 3-phase capacitor bank at bus 675 is switched out. The change in the positive sequence apparent power, as it can be seen, is zero.

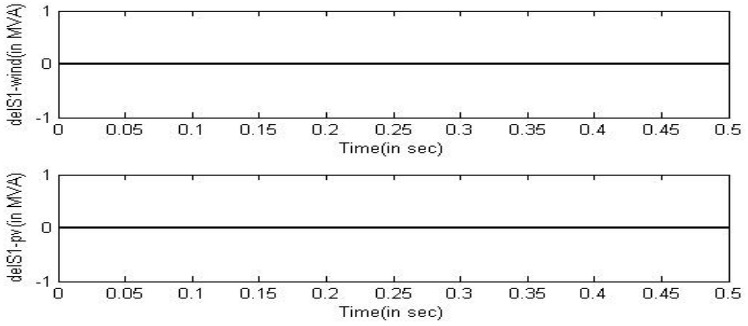

FIGURE 6.43: Positive sequence apparent power difference(in MVA) for capacitor switching

Fig.6.43 shows the result for when a 3-phase load near the PV system is switched out. The change in the apparent power is negligible when compared to the islanding event. The results from these two figures, helps in distinguishing islanding from other events. Thus the product of the difference in voltage and current phasors, which is named here as positive sequence apparent power, can be taken as a reliable parameter for the detection of islanding operation.

6.3 Adaptive Relay Setting

In this section, the final relay settings which are obtained for the two different configurations are shown. Two different system configurations are used. One in which the switch between relay 1.2 and 2.2 is open and the second one in which the switch is closed. C1 being the former configuration and C2 the later.

TABLE 6.1: My caption

Primary Relay			Backup Relay		
Relay ID	Fault Current (in Amp)		Relay ID	Fault Current (in Amp)	
	C1	C2		C1	C2
R1	11547	11547	NA	NA	NA
R2	9145	9145	R4	4212	4048
R2			R8	1866	2212
R3	10200	10404	R1	1129	1130
R3			R8	1739	2008
R4	10640	11490	R6	NA	1080
R5	13790	13600	R3	3692	3419
R6	NA	2350	R12	NA	2345
R7	12015	11890	R1	1120	1115
R7			R4	3849	3668
R8	2510	3845	R10	NA	1595
R9	6470	6380	R7	4140	4025
R10	NA	2894	R11	NA	2894
R11	NA	3580	R5	NA	3580
R12	NA	2782	R9	NA	2782

A close in 3 phase short circuit fault is simulated at different relays. The values of the fault currents are shown in Table.6.1. The table shows the fault currents for both the configurations. The current shown is both for the primary and the backup relays. For different primary relays, there are different relays acting as backup. The limits for pick up current was set between 1.5A and 5A. PSO technique was used for optimization of the relay settings.

TABLE 6.2: Optimal Relay Settings

Relay ID	SG1(k=1)		SG2(k=2)	
	PS	TD	PS	TD
R1	3.420	0.1	3.982	0.1
R2	1.500	0.1	1.500	0.1
R3	2.888	0.1	4.568	0.1
R4	3.937	0.1	4.350	0.1
R5	1.5	0.1	5	0.178
R6	NA	NA	1.740	0.1
R7	3.665	0.1	5	0.112
R8	1.745	0.1	2.268	0.1
R9	1.5	0.1	5	0.132
R10	NA	NA	2.98	0.1
R11	NA	NA	5	0.189
R12	NA	NA	5	0.150
Objective Function(s)	6.483		14.812	

Table.6.2 shows the optimized relay settings obtained at the end of optimization process. The table also shows the final value of the objective function for both configurations. SG1 and SG2 are the relay settings group 1 and 2 corresponding to the two configurations.

Chapter 7

Conclusion

In this work various issues, arising due to the integration of renewable energy sources, are addressed. . High impedance fault detection by analyzing the variation in 3rd harmonic component of current is implemented. In addition to this, mathematical morphology is used for the detection of high impedance fault. 5th harmonic current components are also analyzed and it is concluded that they can also be used for the detection of high impedance fault. A technique based on calculation of the fundamental apparent power is implemented for the determination of fault direction. The fault detection technique is shown to distinguish between an high impedance fault and conditions of capacitor and load switching.

A technique based on the product of change in positive sequence voltage and current is used to detect un-controlled islanding operations. This parameter is used for distinguishing islanding from load and capacitor switching.

An adaptive protection scheme for systems with DG integration is implemented to negate the effect of blinding and sympathetic tripping. The relay settings are determined using non-linear optimization technique. Particle Swarm Optimization was used for the same.

To validate the proposed technique a micro grid environment is simulated in real time using RTDS (Real time digital simulator). For this purpose a typical IEEE 13 bus system is used. In the simulated system wind and solar energy systems are integrated to the grid. A DFIG wind system has been used for the grid integration

Bibliography

[1] Keng-Yu Lien, Shi-Lin Chen, Ching-Jung Liao, Tzong-Yih Guo, Tsair-Ming Lin and Jer-Sheng Shen, "Energy variance criterion and threshold tuning scheme for high impedance fault detection," in *IEEE Transactions on Power Delivery,* vol. 14, no. 3, pp. 810-817, Jul 1999.

[2] A. E. Emanuel, D. Cyganski, J. A. Orr, S. Shiller and E. M. Gulachenski, "High impedance fault arcing on sandy soil in 15 kV distribution feeders: contributions to the evaluation of the low frequency spectrum," in *IEEE Transactions on Power Delivery,* vol. 5, no. 2, pp. 676-686, Apr 1990.

[3] D. I. Jeerings and J. R. Linders, "A practical protective relay for down-conductor faults," in *IEEE Transactions on Power Delivery,* vol. 6, no. 2, pp. 565-574, Apr 1991.

[4] D. C. Yu and S. H. Khan, "An adaptive high and low impedance fault detection method," in *IEEE Transactions on Power Delivery,* vol. 9, no. 4, pp. 1812-1821, Oct 1994.

[5] M. Aucoin and B. D. Russell, "Detection of Distribution High Impedance Faults Using Burst Noise Signals near 60 HZ," in *IEEE Transactions on Power Delivery,* vol. 2, no. 2, pp. 342-348, April 1987.

[6] Detection of high impedance faults, Power Technologies Inc., EPRI Report EL-2413, Jun. 1982.

[7] High Impedance Fault Detection Using Third Harmonic Current, Hughes Aircraft Co., EPRI Report EL-2430, Jun. 1982.

[8] M. Aucoin, B. D. Russell and C. L. Benner, "High impedance fault detection for industrial power systems," in *Industry Applications Society Annual Meeting, 1989., Conference Record of the 1989 IEEE,,*San Diego, CA, USA, 1989, pp. 1788-1792 vol.2.

[9] Detection of arcing faults on distribution feeders, Texas A&M Univ., EPRI Report EL-2757, Dec. 1982.

[10] J. Carr, "Detection of High Impedance Faults on Multi-Grounded Primary Distribution Systems," in *IEEE Transactions on Power Apparatus and Systems,* vol. PAS-100, no. 4, pp. 2008-2016, April 1981.

[11] R. E. Lee and M. T. Bishop, "Performance Testing of the Ratio Ground Relay on a Four-Wire Distribution Feeder," in *IEEE Power Engineering Review,*vol. PER-3, no. 9, pp. 28-29, Sept. 1983.

[12] A. F. Sultan, G. W. Swift and D. J. Fedirchuk, "Detecting arcing downed-wires using fault current flicker and half-cycle asymmetry," in *IEEE Transactions on Power Delivery,*vol. 9, no. 1, pp. 461-470, Jan 1994.

[13] A. V. Mamishev, B. D. Russell and C. L. Benner, "Analysis of high impedance faults using fractal techniques," in *Power Industry Computer Application Conference, 1995. Conference Proceedings., 1995 IEEE,*pp. 401-406, 1995.

[14] I. Zamora, A. J. Mazon, K. J. Sagastabeitia and J. J. Zamora, "New methods for detecting low current faults in electrical distribution systems," in *IEEE Transactions on Power Delivery,*vol. 22, no. 4, pp. 2072-2079, Oct. 2007.

[15] David Chan Tat Wai and Xia Yibin, "A novel technique for high impedance fault identification," in *IEEE Transactions on Power Delivery,*vol. 13, no. 3, pp. 738-744, Jul 1998.

[16] Shyh-Jier Huang and Cheng-Tao Hsieh, "High-impedance fault detection utilizing a Morlet wavelet transform approach," in *IEEE Transactions on Power Delivery,*vol. 14, no. 4, pp. 1401-1410, Oct 1999.

[17] T. M. Lai, L. A. Snider, E. Lo and D. Sutanto, "High-impedance fault detection using discrete wavelet transform and frequency range and RMS conversion," in *IEEE Transactions on Power Delivery,*vol. 20, no. 1, pp. 397-407, Jan. 2005.

[18] M. Michalik, W. Rebizant, M. Lukowicz, Seung-Jae Lee and Sang-Hee Kang, "High-impedance fault detection in distribution networks with use of wavelet-based algorithm," in *IEEE Transactions on Power Delivery,*vol. 21, no. 4, pp. 1793-1802, Oct. 2006.

[19] N. I. Elkalashy, M. Lehtonen, H. A. Darwish, M. A. Izzularab and A. m. I. Taalab, "Modeling and experimental verification of high impedance arcing fault in medium voltage networks," in *IEEE Transactions on Dielectrics and Electrical Insulation,* vol. 14, no. 2, pp. 375-383, April 2007.

[20] N. I. Elkalashy, M. Lehtonen, H. A. Darwish, A. M. I. Taalab and M. A. Izzularab, "DWT-Based Detection and Transient Power Direction-Based Location of High-Impedance Faults Due to Leaning Trees in Unearthed MV Networks," in *IEEE Transactions on Power Delivery,* vol. 23, no. 1, pp. 94-101, Jan. 2008.

[21] C. J. Kim and B. D. Russell, "High-impedance fault detection system using an adaptive element model," in *IEE Proceedings C- Generation, Transmission and Distribution,* vol. 140, no. 2, pp. 153-159, March 1993.

[22] B. D. Russell and C. L. Benner, "Arcing fault detection for distribution feeders: security assessment in long term field trials," in *IEEE Transactions on Power Delivery,* vol. 10, no. 2, pp. 676-683, Apr 1995.

[23] C. L. Benner and B. D. Russell, "Practical high-impedance fault detection on distribution feeders," in *IEEE Transactions on Industry Applications,* vol. 33, no. 3, pp. 635-640, May/Jun 1997.

[24] A. A. Girgis, W. Chang and E. B. Makram, "Analysis of high-impedance fault generated signals using a Kalman filtering approach," in *IEEE Transactions on Power Delivery,* vol. 5, no. 4, pp. 1714-1724, Oct 1990.

[25] Samantaray, S R, Dash, P K, "High impedance fault detection in distribution Feeders using Extended Kalman Filter and Support Vector Machine," in *European Transactions on Electrical Power,* 2009.

[26] M. M. Eissa, G. M. A. Sowilam and A. M. Sharaf, "A New Protection Detection Technique for High Impedance Fault Using Neural Network," in *2006 Large Engineering Systems Conference on Power Engineering,* Halifax, NS, Canada, 2006, pp.-146-151.

[27] H.K.Zadeh, "ANN based high impedance fault detection scheme: design and implementation," in *International Journal of Emerging Electric Power Systems,* vol.4, no.2, pp.1-14,2005.

[28] M. Michalik, M. Lukowicz, W. Rebizant, S. J. Lee and S. H. Kang, "New ANN-Based Algorithms for Detecting HIFs in Multigrounded MV Networks," in *IEEE Transactions on Power Delivery,* vol. 23, no. 1, pp. 58-66, Jan. 2008.

[29] Gautam, S, Brahma, S.M., "Detection of high impedance fault in power distribution systems using mathematical morphology," in *IEEE Transactions in Power Systems,* vol. 28, no. 2, pp. 1226-1234, May. 2013.

[30] Gautam, S, Brahma, S.M., "Overview of mathematical morphology in power systems- A tutorial Approach," in *Power & Energy Society General Meeting, 2009. PES'09. IEEE,* vol.,no., pp.1-7,26-30 July 2009.

[31] R. A. Walling, R. Saint, R. C. Dugan, J. Burke and L. A. Kojovic, "Summary of Distributed Resources Impact on Power Delivery Systems," in *IEEE Transactions on Power Delivery* vol. 23, no. 3, pp. 1636-1644, July 2008.

[32] B. Hussain, S. M. Sharkh, S. Hussain and M. A. Abusara, "Integration of distributed generation into the grid: Protection challenges and solutions," *Developments in Power System Protection(DPSP 2010). Managing the Change, 10th IET International Conference on,* Manchester, 2010, pp. 1-5.

[33] Kyle I. Jennett, Campbell D. Booth, Federico Coffele and Andrew J. Roscoe, "Investigation of sympathetic tripping problem in power systems with large penetration of distributed generation," *IET Generation Transmission Distribution,* vol.9, no.4,pp.379-385, Mar 2015.

[34] C. J. Mozina, "Impact of Green Power Distributed Generation," in *IEEE Industry Applications Magazine,* vol. 16, no. 4, pp. 55-62, July-Aug. 2010.

[35] P. Mahat, Z. Chen, B. Bak-Jensen and C. L. Bak, "A simple adaptive overcurrent protection of distribution systems with distributed generation," in *IEEE Transactions on Smart Grid,* vol. 2, no. 3, pp. 428-437, Sept. 2011.

[36] M. M. Mansour, S. F. Mekhamer and N. El-Kharbawe, "A modified particle swarm optimizer for the coordination of directional overcurrent relays," in *IEEE Transactions on Power Delivery,* vol. 22, no. 3, pp. 1400-1410, July 2007.

[37] V. A. Papaspiliotopoulos; G. N. Korres; V. A. Kleftakis, "Hardware in the loop design and optimal setting of adaptive protection schemes for distribution systems with distributed generation," in *IEEE Transactions on Power Delivery,* vol.PP, no.99, pp.1-1.

[38] L. K. Kumpulainen and K. T. Kauhaniemi, "Analysis of the impact of distributed generation on automatic reclosing," in *Power Systems Conference and Exposition,2004. IEEE PES,*2004, pp. 603-608 vol.1.

[39] S. Phuttapatimok, A. Sangswang, M. Seapan, D. Chenvidhya and K. Kirtikara, "Evaluation of fault contribution in the presence of PV grid-connected systems," *Photovoltaic Specialists Conference,2008. PVSC'08. 33rd IEEE,* San Diego, CA, USA, 2008, pp. 1-5.

[40] R. A. Walling and N. W. Miller, "Distributed generation islanding-implications on power system dynamic performance," *Power Engineering Society Summer Meeting,2002 IEEE,* Chicago, IL, USA, 2002, pp. 92-96 vol.1.

[41] M. A. Redfern, O. Usta and G. Fielding, "Protection against loss of utility grid supply for a dispersed storage and generation unit," in *IEEE transactions on Power Delivery,* vol. 8, no. 3, pp. 948-954, July 1993.

[42] W. Xu, G. Zhang, C. Li, W. Wang, G. Wang and J. Kliber, "A Power Line Signaling Based Technique for Anti-Islanding Protection of Distributed GeneratorsPart I: Scheme and Analysis," in *IEEE transactions on Power Delivery,* vol. 22, no. 3, pp. 1758-1766, July 2007.

[43] S. I. Jang and K. H. Kim, "A new islanding detection algorithm for distributed generations interconnected with utility networks,," *Developments in Power System Protection, 2004, Eighth IEE International Conference on,* 2004, pp. 571-574 Vol.2.

[44] All India installed capacity(in MW) of Power Stations, CEA, India, 30 April 2016.

Appendix

Wind Data

The electrical and mechanical parameters of the wind system are used are given below:

Rated speed= 8 m/s

Rated stator voltage (L-L RMS)= 0.69 KV

Rated Frequency= 50Hz

Stator Resistance= 0.00462 pu

Stator Leakage Reactance= 0.102 pu

Unsaturated Magnetizing Reactance= 4.348 pu

First Cage Rotor Resistance= 0.006 pu

First Cage Rotor Leakage Reactance= 0.08596 pu

Inertia Constant= 1.5 MWs/MVA

Solar data

Rated temperature= $10000°C$

Rated Solar intensity= 1000 W/m2

Open circuit voltage= 21.7 V

Short circuit current= 3.35 A

Voltage at maximum power= 17.4 V

Current at maximum power= 3.05 A

Transformer Data

4.16KV/0.563 KV, wye-wye transformer

Rated MVA= 0.5 MVA

Base Frequency= 50Hz

Leakage Inductance= 0.0408 pu